A SYSTEMS APPROACH TO MODELLING AND DESIGN OF HIGH STRAIN SHAPE MEMORY ALLOY ACTUATORS

Xuemei Lu

Department of Electrical Engineering
McGill University

September 1997

A Thesis submitted to the Faculty of Graduate Studies and Research
in partial fulfilment of the requirements for the degree of
Master of Engineering

0-612-37267-7

Abstract

A simulator is developed to model and design high strain shape memory alloy (SMA) tension actuators. The simulator may be used to predict characteristics of a given actuator, or to design its geometry under specifications such as force, speed, stroke and size. The accuracy of the model is verified experimentally in reference to an existing NiTi shape memory alloy prototype actuator. Having developed some confidence in the model, the performance of the proposed actuation mechanism is compared to other existing technologies. In particular, the force-displacement and speed characteristics of a micro-solenoid electro-magnetic actuator and a muscle-size pneumatic actuator are compared to those of the SMA actuators with same dimensions.

A new concept of designing shape memory alloy bending actuator is presented in the end of the thesis. Part of the modelling work is accomplished in this research by developing a software simulator which is capable of predicting the geometric transformation of the actuator during bending. As a result, the dynamic strain of each SMA fiber in the actuator can be computed given a bending axis and angle. Graphical display of the bending transformation is implemented using in house software package. Further investigation of modelling and control of the SMA bending actuator is left as future work.

Résumé

Dans cette thèse, on dévelope un modèle, puis un simulateur informatique d'actionneurs à mémoire de forme à grande course. Le simulateur peut prédire les caractéristiques d'un actionneur donné ou servir à dimensionner un actionneur selon des spécifications telles que la force, la vitesse, la course et la taille. Une validation expérimentale du simulateur et du modèle est faite en référence à un actionneur déjà disponible. Ayant gagné une certaine confiance dans le modèle, la performance d'actionneurs de ce type est comparée à celles d'autres technologies. On compare en particulier la performance de ces actionneurs à mémoire de forme à celles d'un micro-solenoïde électromécanique et à celles d'un actionneur pneumatique à chambre élastique.

Un nouveau concept d'actionneur à mémoire de forme qui travaille en flexion est aussi présenté. La modélisation de cet actionneur est faite en spécifiant ses propriété géométriques au simulateur. Ceci permet de calculer l'étirement de chaque fibre étant donné un angle de flexion. Les résultats sont présentés de façon infographique. Une modélisation plus détaillée et la commande de ce nouvel actionneur pourra faire l'objet de travaux ultérieurs.

Acknowledgements

A thesis is rarely conceived in isolation. This work is certainly no exception. First of all, I would like to thank my supervisor Vincent Hayward, whose helpful insight and advice proved crucial to the completion of this research. His guidance and patience have been appreciated.

Theoretical results are always best confirmed by experiments. Without the assistance of Danny Grant, the experimental results would not have been possible.

I would also like to thank Gilbert Soucy whose expertise in computer graphics and software engineering aided me in developing the 3D graphical display program for the shape memory alloy actuator.

Thanks also go to the many people who helped to maintain my sanity during these academic years, especially Hamid Taghirad, Michael Glaum, Kenong Wu, Juan Manuel Cruz, Mordechai and Noga Arenson.

My parents, Qian Lu and Ya Mei, have contributed immensely to my entire life, especially during the time of my studying in Canada.

Finally, I wish to acknowledge my boyfriend, Thomas Lee, who has consistently paid attention to discussion of problems in the thesis, and shared my moments of elation and frustration. His encouragement and support are valuable.

TABLE OF CONTENTS

LIST OF FIGURES

Claim of Originality

The author of this thesis claims the following original contributions:

- the design of the software simulator for NiTi shape memory alloy actuator.
- the design of the shape memory alloy bending actuator prototype.
- the design of the software simulator for modelling the geometric transformation of the prototype SMA bending actuator.

CHAPTER 1

Introduction

1. Overview

The research of this thesis involves the investigation of mechanical and thermal properties of certain nickel and titanium (Ni-Ti) based *shape memory alloys* (SMA). A mathematical model of SMA properties useful for designing micro actuators is developed. The model of a novel SMA tension actuator is created and the accuracy of this model is verified experimentally in reference to an existing NiTi shape memory alloy prototype actuator. A new concept for making SMA bending actuators is proposed and simulated.

Chapter 2 of the thesis gives some background information on the applications of shape memory alloy actuators as well as a brief literature review on the modelling aspect. The distinguishing mechanical characteristics of shape memory alloys are detailed in Chapter 3, in which the mathematical model of a particular type of SMA fiber is constructed based on Ikuta's variable sublayer approach [1] proposed in 1991. An application of this model to the analysis and design of SMA tension actuators is seen in Chapter 4. Chapter 5 explores a new strategy for building miniature SMA bending actuators. Further discussions of the simulation results are presented in conclusion in Chapter 6.

2. The Shape Memory Effect

Shape memory effect (SME) refers to the ability of certain novel materials to recover a predetermined shape when heated [2]. When a SMA is in *Martensitic phase* (M-phase) at low temperature, it has a very low yield strength and can be deformed quite easily into a new shape, which it retains. However, when the material is heated so that it is in *Parent phase* (P-phase), also called Austenic phase at high temperature, the alloy undergoes a change in crystal structure which causes it to return to its original shape. If the SMA is loaded during this transformation, it can generate extremely large forces. This phenomenon provides an unique mechanism for actuation.

The phase transformations between Martensite and Austenite are characterized by four transformation temperatures [2]. Namely,

(i) M_s, the Martensite starting temperature,
(ii) M_f, the Martensite finishing temperature,
(iii) A_s, the Austenite starting temperature,
(iv) A_f, the Austenite finishing temperature.

An illustration of the shape memory effect is shown in Figure 1.1. There is no change in the shape of a specimen cooled from a temperature above A_f to below M_f. When the specimen is deformed below M_f, it retains the deformation until it is heated. The shape recovery begins at A_s and is completed at A_f. Upon this, the shape memory can only be reactivated by deforming the Martensitic specimen once again. In other words, the shape memory effect is a one time only occurrence and because of this it is frequently referred to as *one-way shape memory* [2].

3. The Phase Transformation

Shape memory alloys show distinct physical properties at different phases as shown in Figure 1.2. This behaviour is caused by the transformation of material

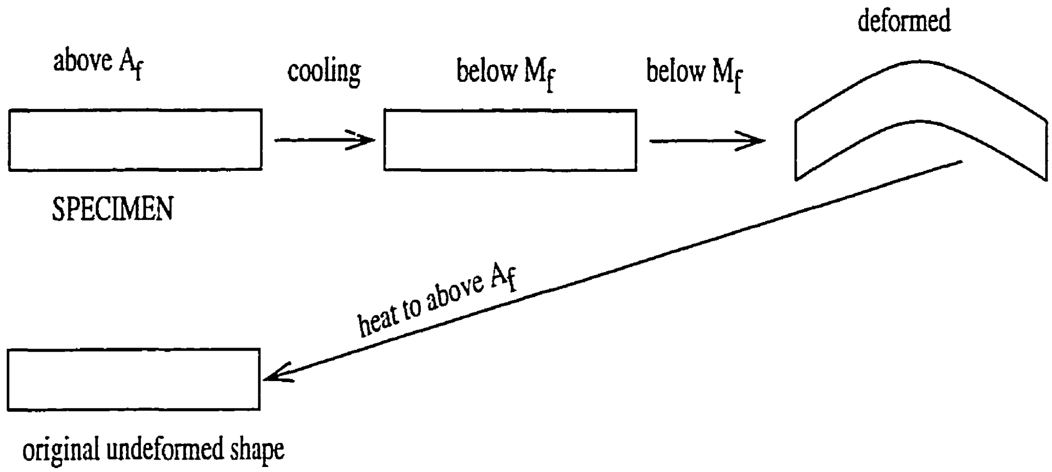

FIGURE 1.1. The Illustration of Shape Memory Effect.

lattice structures during phase transitions. For an exploration of the microscopic phenomenon refer to [2].

It can be seen from Figure 1.2 that the temperature induced phase transformation results in a corresponding change in the physical attributes such as electrical resistance, length and volume of the alloy. Moreover, it is possible to control the temperature of SMA by means of electrical current input. These unique characteristics have attracted much attention from various fields in industry [3] [4] [5].

3.1. Martensite. When the temperature is below M_f, the shape memory alloy is under 100% Martensite. Figure 1.3 illustrates the typical stress-strain relationship of SMA in M-phase. The linear portion of the curve prior to point A corresponds to the elastic region in which the material returns to the original shape when the stress is released. This property is common among metals.

Since the Martensitic alloy is quite malleable, a large external stress can mechanically change the internal structure of a sample, which results in a substantial deformation with only a very small increase in stress. Hence, a plateau occurs in the stress-strain curve as shown in Figure 1.3, between points A and B. If the external stress is removed in this range, the shape of the sample will recover slightly

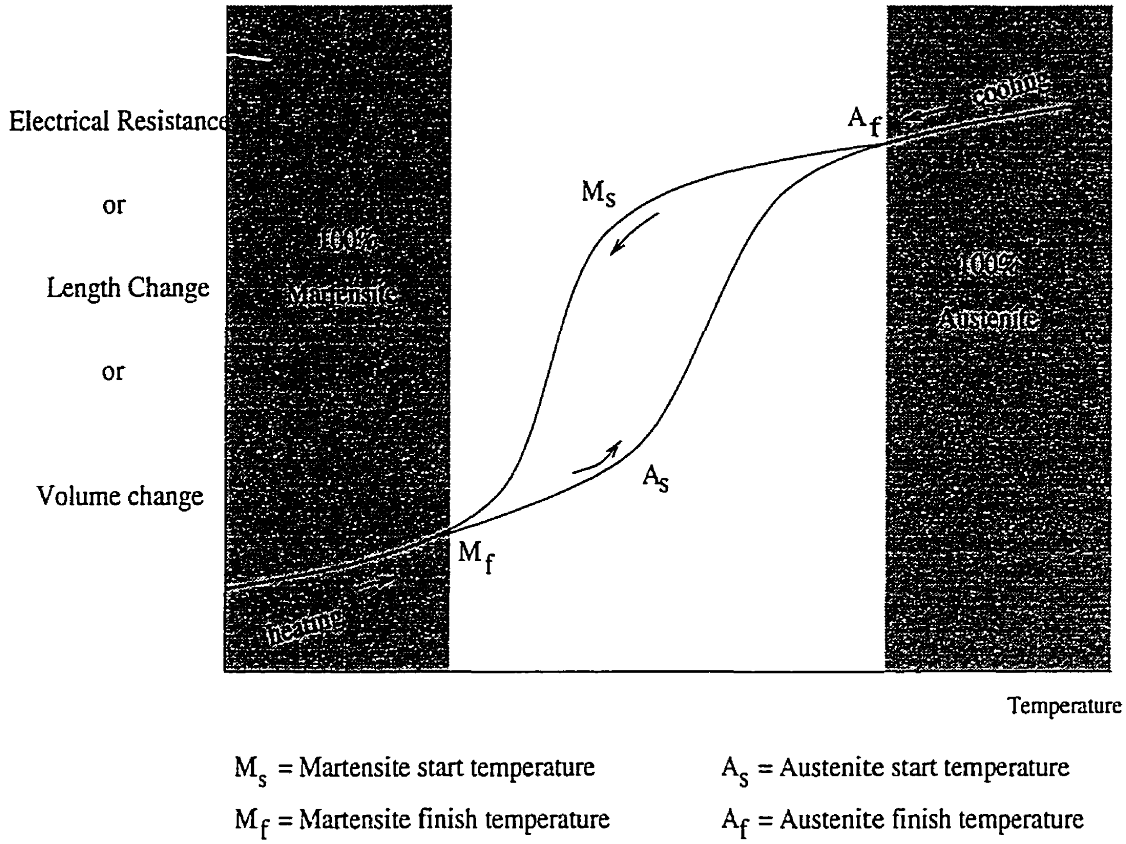

FIGURE 1.2. Temperature Dependence of Physical Properties

but remain deformed. This is similar to plastic deformation, except that with shape memory alloy, the original shape can be fully retrieved by heating.

When the alloy sample is stretched between points B and C in Figure 1.3, it exhibits elastic behaviour again. If the stress is released in this region, the SMA will return to its already deformed shape as indicated in the figure by the dotted line.

If further stress is applied after point C in the curve, the atomic bonds of the material will be broken and the alloy will be permanently deformed.

3.2. Stress-induced Martensite. It is well known that the phase transformation of the shape memory alloy is not only dependent on the temperature, but also on the external stress.

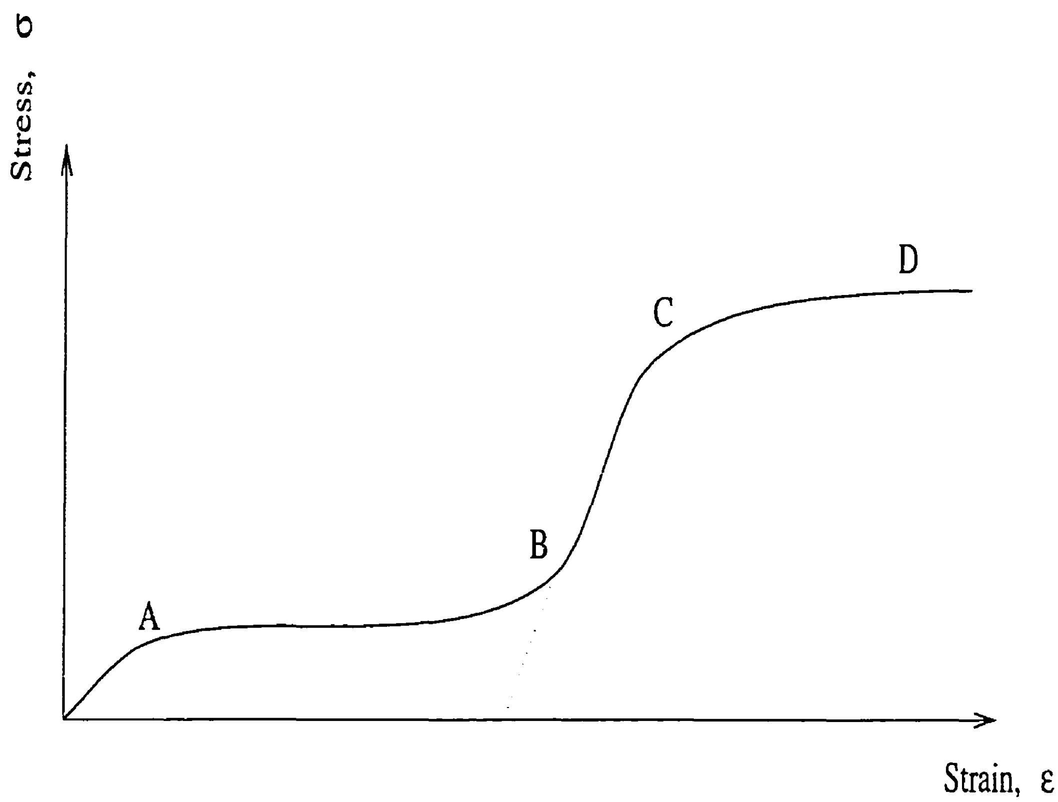

FIGURE 1.3. Typical Stress-strain Relationship of Martensite

In an unloaded SMA sample, the Martensite formation begins when the temperature falls below M_s. However, it is possible to induce Martensite formation above M_s by applying sufficient stress to the alloy. The applied stress mechanically transforms the Austenite crystal lattice into that of the Martensite. Martensite formation caused by external stress is known as *stress-induced martensite* (SIM).

Figure 1.4 illustrates how the Martensite starting temperature M_s of the shape memory alloy shifts with increasing external stress. The other transformation temperatures move in the same fashion. Since the mechanical properties of Martensite and Austenite are completely different, it is clear that any applications of shape memory alloys involving external loads should take into account the effect of the stress-induced Martensite. It has been found that there is a well-defined relationship between the temperature and the stress required to induce Martensite formation. More of this will be discussed in the modelling of SMA properties in chapter three.

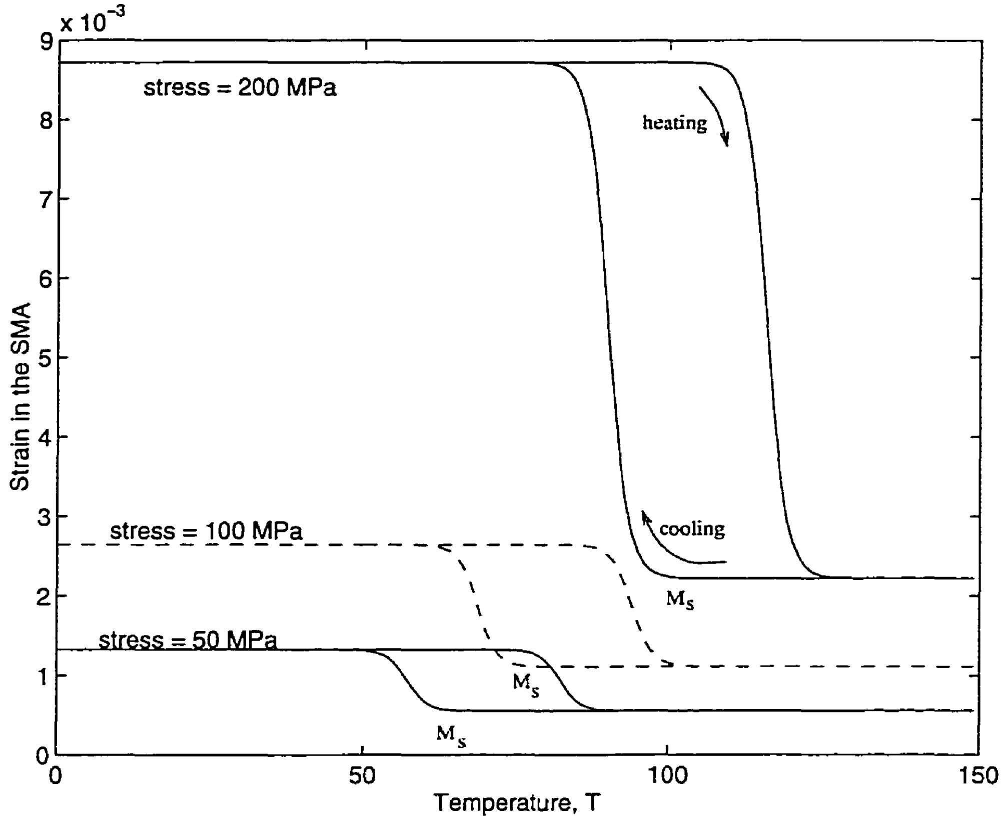

FIGURE 1.4. Illustration of the Stress Induced Martensite

3.3. Austenite. The shape memory alloy is in Austenite phase if its temperature is above A_f. As shown in Figure 1.5, the Austenite SMA is rigid, exhibits properties similar to those of steel or standard piano wire. It behaves elastically up to a certain level of applied stress (stage A in Figure 1.5). If greater stress is applied, in stage B the alloy will be permanent deformed or damaged, heating will not return to the original shape, following stage C.

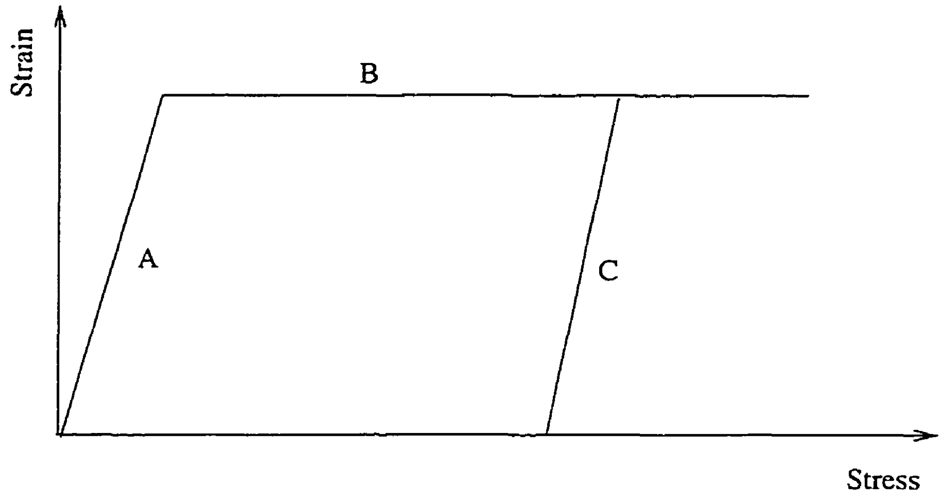

FIGURE 1.5. Stress-strain Relationship of Austenite

CHAPTER 2

Background

The shape memory effect in alloys was first discovered by the Swedish physicist Arne Olander in 1932 using an alloy of gold and cadmium. Since then, many materials have been found to exhibit such properties. The most common is an alloy of nickel and titanium called Nitinol (NiTi). This particular alloy has very good electrical and mechanical properties, long fatigue life, and high corrosion resistance. As an actuator, it is capable of up to 5% strain recovery and 180 Mpa stress restoration with many cycles [**6**]. NiTi also has resistance properties which enable it to be heated electrically. Honma, Miwa and Iguchi [**7**] demonstrated that the phase transitions of the NiTi shape memory is controllable by electric heating, which makes them effective in micro-robotics.

Over the past decade, the interest in making actuators with shape memory alloy has been increasing [**6, 2, 8**]. Conventional technologies such as electric, hydraulic, and pneumatic actuators have difficulties generating significant power when their size and weight are scaled down [**3**]. If the weight requirement of an actuator is 100 grams or lighter, even DC motors can not exceed the power to weight level of 10 [W/kg]. Shape memory alloy actuators however, can attain a high power to weight ratio of almost 100 [W/kg]. Since the actuation of SMA is based on strain energy, its advantages are more evident in miniature application.

1. Advantages and Limitations of Shape Memory Alloy Actuators

In addition to the high power to weight ratio, shape memory alloy has several other advantages for miniaturization. First of all, the actuation mechanism is simple. Similar to pneumatic or hydraulic actuation, the stress by cross-sectional area is sufficiently high to allow for direct drive, for using phase transformation of the alloy to convert thermal energy into mechanical form. Therefore, force or torque amplification systems such as gears or screws are not required. In fact the opposite is often needed: displacement amplification. This observation led to the design introduced by Grant and Hayward (see Chapter 3). Secondly, shape memory alloy applied to miniature actuators in well selected cases, should lead to reduced production cost and improved reliability. The cleanliness condition of SMA as well as bio-compatibility makes it possible for medical surgery, biotechnology, and microelectronics applications. Silent actuation is another important feature of this approach.

Nevertheless, shape memory alloy actuators also come with several limitations. Generally, the SMA actuators are inferior to others in energy efficiency and fatigue life regardless of the scale. Furthermore, the dynamic range of the NiTi shape memory alloy is limited to approximately 8% absolute strain, while in practical applications the strain is often restricted to around 5% or less. The life time of the alloy has also been found to dramatically increase if the fiber is operated at lower absolute strain [3]. Hunter et al. [8] reported that the cycle lifetime of a NiTi shape memory alloy sample at a strain of 5% is about 10^5. Another major complaint about shape memory alloy actuators is the large time constant in natural cooling that makes the wire slow to relax. However, the surface area to volume ratio increases as wire size decreases, therefore the disadvantage of slow cooling is less pronounced in miniature scale.

2. Application of Shape Memory Alloy Actuators

Extensive research has been carried out to find practical applications for shape memory alloys [**2, 9, 10**]. One category of interest concerns with applying SMA actuators in Endosurgery [**11, 12, 13, 14**]. Other application fields involve various micro-robotics research [**8, 15, 16**]. Examples of commercial shape memory actuation devices include pipe couplings, electrical connectors, coffee-pot thermostats, damping devices, glove hammer, etc. Except for the thermostat application, very few of these applications take advantage of the actuating properties of SMAs.

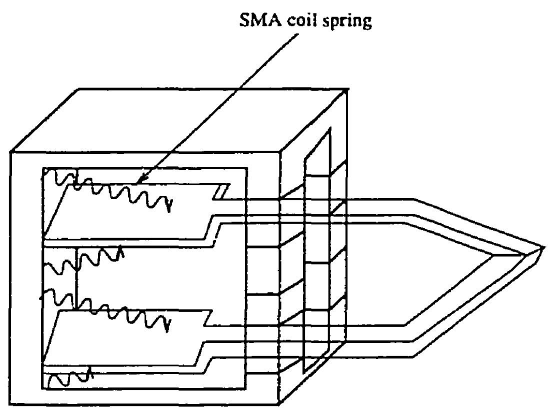

FIGURE 2.1. Miniature Clean Gripper Actuated by SMA

Devices actuated by SMA in coil shape is one popular method to make shape memory alloy actuators. Figure 2.1 gives an example of a miniature clean gripper designed by Ikuta [**3**] using SMA spring coils. Although SMA in coil form can effectively achieve motion amplification, it often requires large diameter SMA fiber to produce enough power. This is negative for the response time since the time constant of a SMA wire is proportional to its diameter. Other SMA actuator designs include using straight or curvature shape memory alloy fibers. They both depend on increasing the size of the actuators in order to amplify the mechanical motion. We will see in Chapter 4 how this problem was solved by Grant and Hayward.

3. Modelling

Even though a substantial amount of work has been concerned with establishing mathematical models for shape memory alloys, most conventional models existing in the literature study the behaviour of SMA from a material science point of view [**17**, **18**]. They are not suitable for systems engineers for use them in controller design because these methods must be put in form suitable for systems analysis and design, which is one topic of this thesis. Linear models proposed by Hashimoto et al. [**19**] and by Kuribayashi [**20**] all make the crude assumption that the shape memory behaviour is linear and ignore the hysteresis due to phase transition. While such an assumption simplifies the controller design, it is only valid for very small dynamic ranges. A reasonably successful nonlinear model was developed by Ikuta et al. [**1**] and extended by Madill [**21**] to account for both major and minor hysteresis behaviour. However, Ikuta's model did not account for switching between major and minor hysteresis loops, while Madill ignored the spring effect existing in shape memory alloy. Few of these models have been used to design SMA actuators and analyze their performance before they are constructed.

In this thesis, modelling is used to describe the shape memory alloy actuator system from different points of view. The characteristics of a SMA actuator system are divided into three groups, namely the thermal property (tp), the material property (mp), and the geometric property (gp). A simulator is designed to model each group and together the overall behaviour of the system.

The overall system can be described by a constitutive equation

$$G(tp, mp, gp, i, \sigma, \epsilon) = 0. \tag{2.1}$$

where i is the current, σ is the stress, and ϵ is the strain of the actuator system.

If sufficient input variables to function are specified, the relation for the rest of the variables is determined. For a specific SMA actuator, the parameters related to thermal property, material property and geometric property are fixed. Therefore, $G = 0$ may be used to characterized the input-output relationship of the system.

Most conventional models deal with this relationship since it is important for controller design. But when designing a specific actuator, stress, strain and some other actuator parameters are given as specifications, while the remaining parameters are to be determined to satisfy the requirements. A particular common version of this problem is to design a SMA actuator given stipulations such as force, stroke, size and material. Conversely, it might be needed to determine desired material properties such as transition temperatures, in order to achieve a certain level of performance given geometrical constraints. In the following chapter, detailed discussion on the strategy and implementation of the actuator model is presented.

CHAPTER 3

Modelling of Shape Memory Alloy Properties

1. Model Structure

The schematic model of the shape memory alloy is depicted in Figure 3.1. The three blocks shown in the figure illustrate the temperature-current relationship, the R_m (Martensite fraction)-temperature relationship, and the strain-stress-R_m relationship of the alloy. A computer simulator is developed to model each individual block and together the overall behaviour of the system.

As seen in the introduction, the shape memory alloy exhibits different mechanical properties at different phases (Martensite, Austenite, or mixture of the two phases). The stress-strain is dependent on the phase of the alloy. The phase of a shape memory alloy is determined by its temperature and by the external stress applied to it. A hysteresis is formed during the phase transformation, due to the fact that the phase transitions follow different curves during heating or cooling. There are various methods to control the temperature of the sample. Two commonly used techniques are electric current input and fluid bath. Submerging a SMA in a fluid bath is convenient for setting its temperature, however, it might not be always practical. In this thesis, Ikuta's variable sublayer concept is used to model the phase transformation of a NiTi

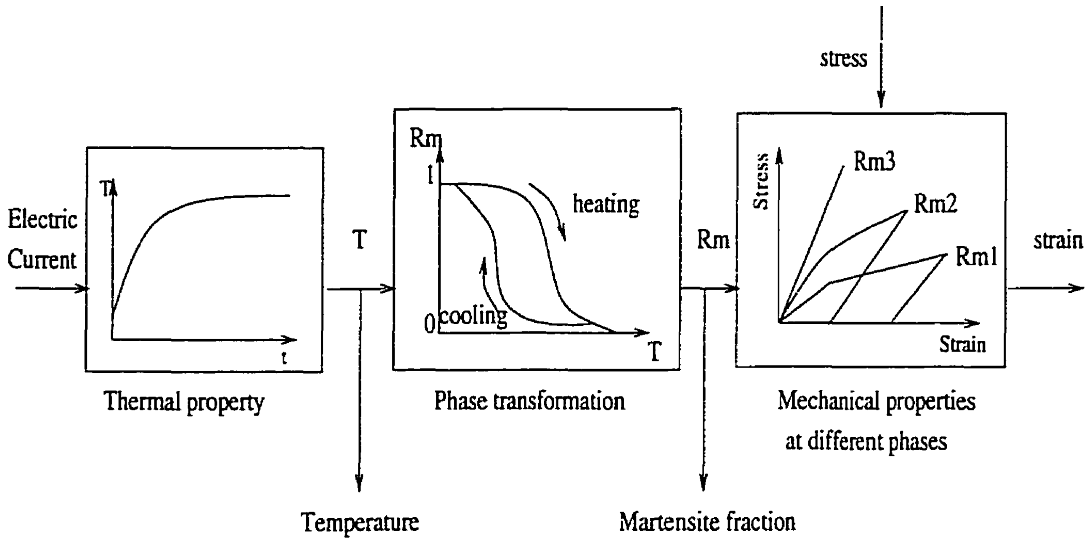

FIGURE 3.1. The Block Diagram of the SMA Model

shape memory alloy, while heating SMA fibers with electric current is used to replace the water bath in Ikuta's experiments.

2. Temperature-Current Relationship

The temperature of the shape memory alloy fiber is difficult to measure due to its small diameter. However, it has been observed that the strain versus time characteristic of a SMA tension actuator was approximately first order when the SMA fibers of the actuator were heated with constant pulse currents [**6**].

From the thermal conduction and heat transfer point of view, the internal heat energy change of the SMA fiber must equal to the energy dissipated in the fiber by electric currents, less the energy transfered to the air by natural convection [**22**]. Mathematically, this can be expressed as:

$$\rho \cdot Cp \cdot V \cdot \frac{dT(t)}{dt} = R \cdot i^2(t) - h \cdot A \cdot (T(t) - T_\infty) \tag{3.1}$$

where

ρ: density of the SMA fiber [kg/m^3]

C_p: heat capacity of the SMA fiber [J/Kg·°C]

V: volume of the SMA fiber [m^3]

T: temperature of the SMA fiber [°C]

t: time [s]

i: electric current [amp]

R: resistance of the SMA fiber [Ω]

h: heat transfer coefficient [W/m^2 °C]

A: surface area of wire [m^2]

T_∞: ambient temperature [°C]

Solving equation 3.1 for T yields:

$$T(t) = Ce^{-at} \int_{-\infty}^{t} e^{a\tau} i^2(\tau) d\tau + C_0 e^{-at} + T_\infty \tag{3.2}$$

where C and a are thermal constants that can be identified experimentally or calculated theoretically as follows:

$$C = \frac{R}{\rho C_p V}, \quad a = \frac{hA}{\rho C_p V} \tag{3.3}$$

C is essentially the dissipation that affects the steady-state value of the temperature, while a is the capacitance which determines the time constant of the system.

Note that these formulae can only provide approximate estimates, being based on a crude heat transfer model. In practice, these constants are preferably identified experimentally. They provide however very valuable information about their trend, when the geometry of the fibers are changed (V and A), all other variables being held constant. Since the rise time of a shape memory alloy is inversely proportional to its capacitance, it can be implied that the response time of a SMA actuator system is proportional to the volume versus surface area ratio of the SMA wire, hence directly related to the wire diameter.

The left side of Figure 3.2 illustrates the time domain open loop response to a set of pulse current applied to a 100μ NiTi shape memory alloy fiber, while the right side of the figure displays the response in detail over a shorter time interval. The

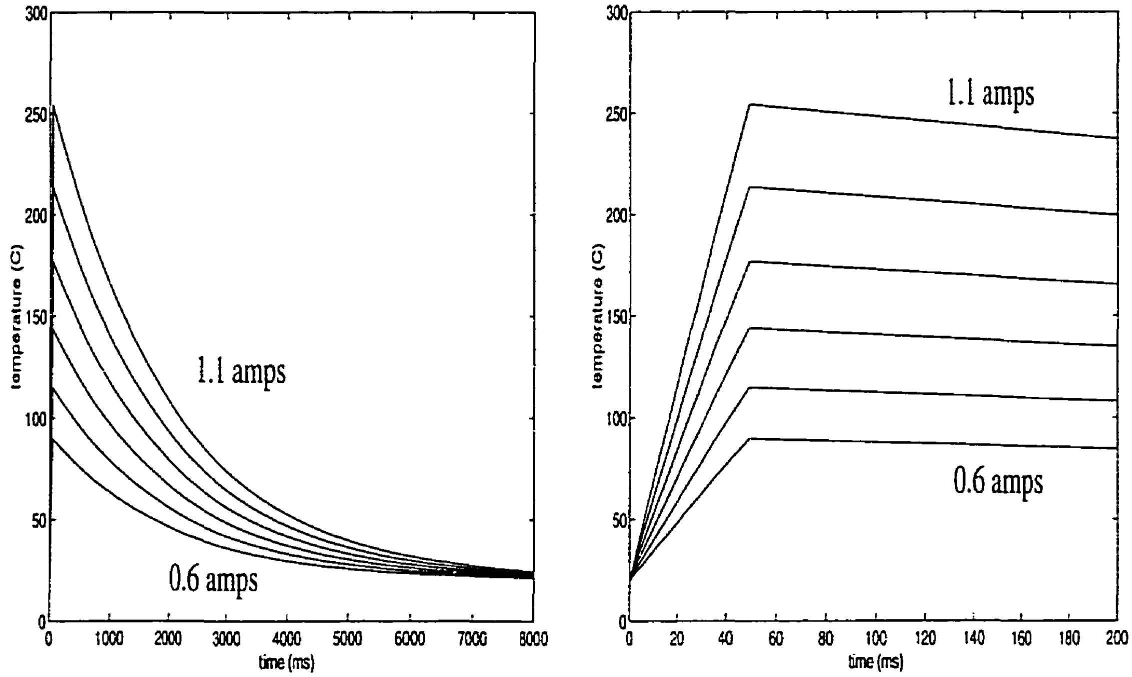

FIGURE 3.2. Temperature-current Relationship of SMA

duration of the pulse is 50 ms, with the amplitude varied from 0.6 amp to 1.1 amp. The thermal constants C and a calculated based on equation (3.3) are 0.66 and 4200.0 respectively. The parameters reflecting various properties of the NiTi shape memory alloy fibers being used are listed in Appendix A. In Grant's research [**6**], a variable structure controller is designed to control the heating of the SMA fibers so that the actuator moves to a desired position quickly and precisely.

3. Phase Transformation

The M-phase and P-phase are the two principal phases of the shape memory alloy. A third phase, known as R-phase has been recently discovered in SMA annealed at low temperature [**23**]. The R-phase transformation has a much smaller hysteresis than that of the Martensitic transformation, but the maximum recoverable strain is only about 1%. Since the R-phase is negligible for shape memory alloys designed to have larger dynamic ranges, the modelling of the phase transformation in this thesis handles only the two principal phases of the alloy to simplify the structure. Nevertheless, it can be easily extended to include the R-phase transformation if necessary.

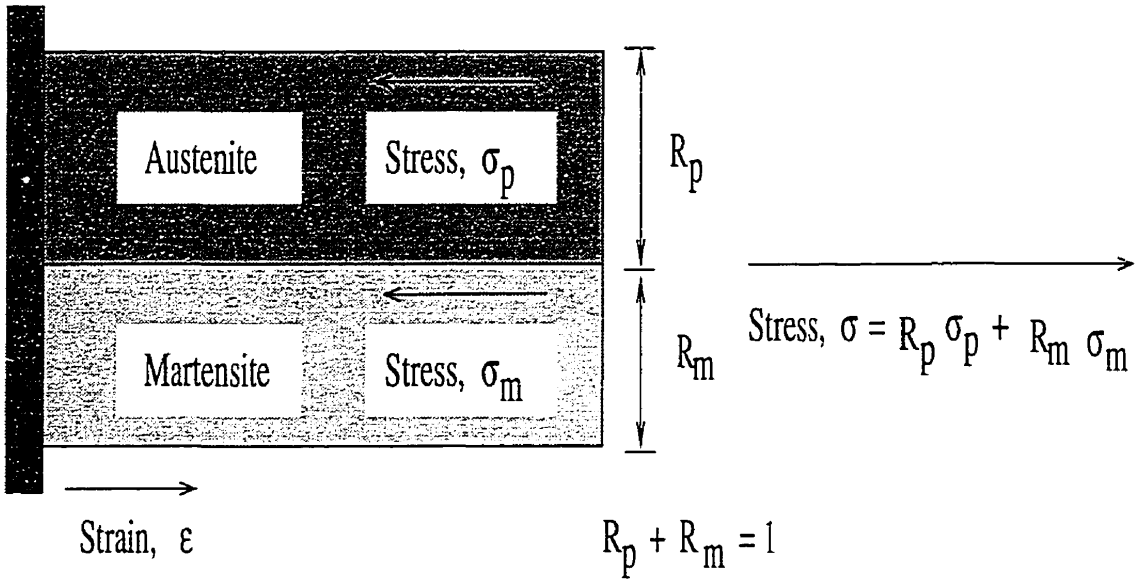

FIGURE 3.3. Variable Sublayer Model

Figure 3.3 describes the basic assumptions of the variable sublayer model of SMA first reported by Ikuta [**3**]. The sublayer model consists of parallel connected sublayers whose mechanical properties are different from each other. The overall mechanical characteristic of the alloy is proportionally contributed by each sublayer according to its phase volume fraction. Let R_m and R_p be the volume fraction of the Martensite and Austenite respectively in a shape memory alloy. The summation of fractions is always 1 in:

$$R_m + R_p = 1 \tag{3.4}$$

A SMA at equilibrium state could be in 100% M-phase ($R_m = 1$), 100% P-phase ($R_p = 1$), or in a phase where both Martensite and Austenite coexist. The phase transitions of a SMA depend on its temperature and the external load applied to it.

3.1. R_m-Temperature Relationship. A generalized transformation hysteresis model is developed by Ikuta [3] to approximate the R_m-Temperature relationship of the NiTi shape memory alloy:

$$R_m(T) = \frac{R_{ma}}{1 + e^{k_m}(T - T_{0m})} + R_{mb} \tag{3.5}$$

R_{ma} and R_{mb} are constants, k_m and T_{0m} take different values for the heating and cooling processes:

- During cooling:

$$\begin{aligned} T_{0m} &= \frac{1}{2(M_s + M_f)} \\ k_m &= \frac{\kappa}{M_s - M_f} \end{aligned} \tag{3.6}$$

- During heating:

$$\begin{aligned} T_{0m} &= \frac{1}{2(A_s + A_f)} \\ k_m &= \frac{\kappa}{A_f - A_s} \end{aligned} \tag{3.7}$$

The constant κ was determined empirically by Ikuta [3] to have a value of 6.2.

Figure 3.4 and 3.5 illustrates the phase transformation hystereses for various R_{ma} and R_{mb}. The condition $R_{ma} = 1$ and $R_{mb} = 0$ characterises the major hysteresis loop in which the switching between heating and cooling processes happens only when the alloy is under pure Martensite or pure Austenite. The minor hysteresis loops can be modelled by adjusting R_{ma} and R_{mb} appropriately. The constant R_{ma} is essentially a gain factor while R_{mb} represents an offset. As shown in Figure 3.4, if the sample is cooled from point 1 at which it is almost entirely Austenite, the Martensite fraction will increase according to the major hysteresis curve defined by $R_{ma} = 1$ (following the arrow along the bottom of the hysteresis). When the wire temperature reaches point 2, 60% of the wire will be Martensite. If the wire is heated from this point instead of being cooled further towards the complete Martensite, the Martensite fraction will

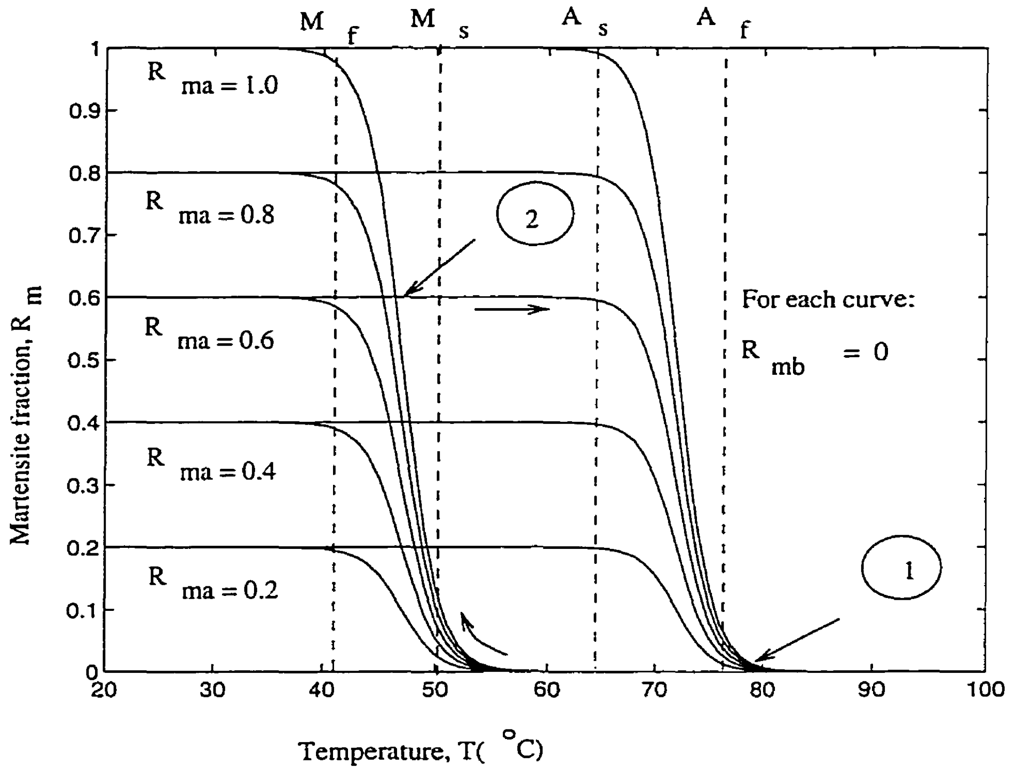

FIGURE 3.4. Martensite Fraction versus Temperature for Various R_{ma} and R_{mb}

then decrease according to the curve defined by $R_{ma} = 0.6$. Similarly, Figure 3.5 gives an example of switching from major loop to minor loop when the heating of the alloy is changed to cooling at point 2.

Ikuta's report [**3**] focused on modelling the major hysteresis loop of the phase transition, while switching between the major and minor loops is not explored. For the model to be useful in simulating control applications, cycling within numerous minor hysteresis loops may be expected. To overcome this limitation, Madill [**21**] extended Ikuta's model to cover minor hysteresis loops by treating R_{ma} and R_{mb} as piecewise-constant functions of time. However, Madill restricted the SMA wire to start either at the ambient temperature or at a temperature above the Austenite finish temperature. Moreover, the formulae and condition described by Madill for adjusting R_{ma} and R_{mb} during switching are complicated for computer implementation.

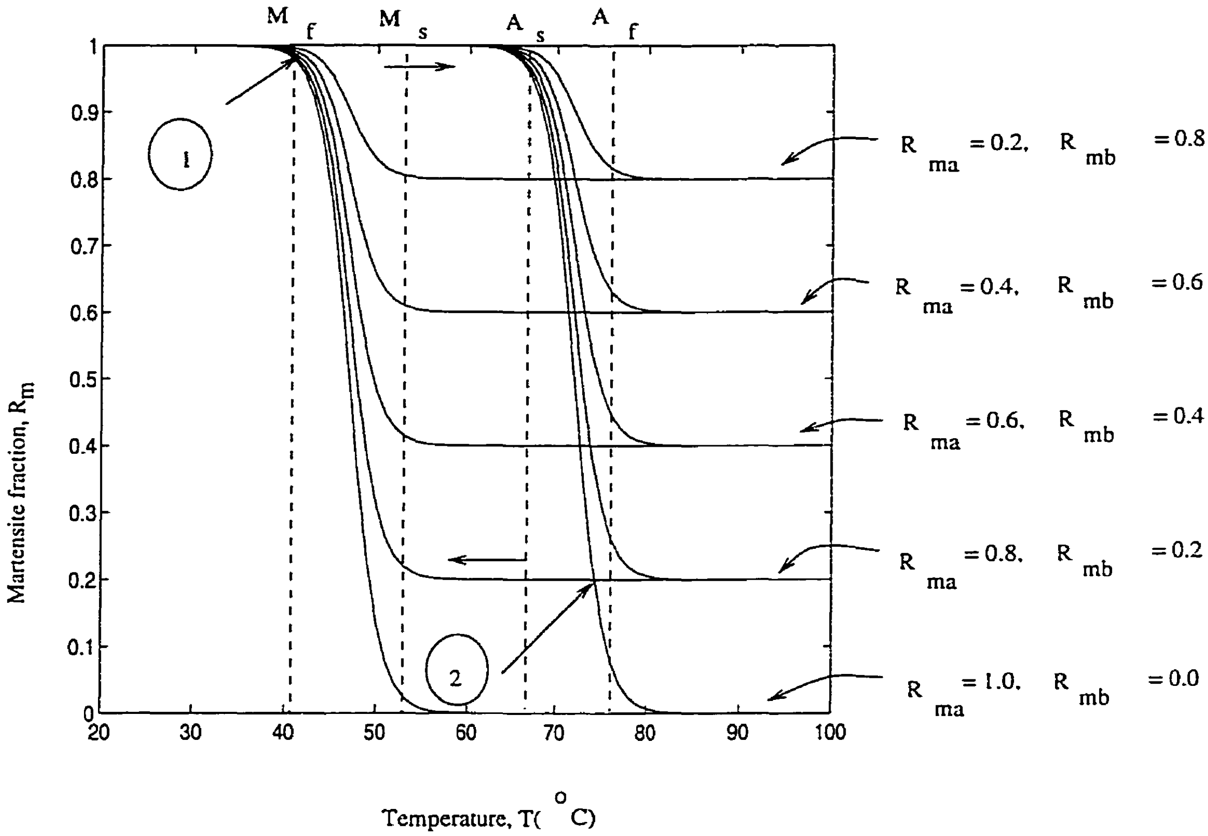

FIGURE 3.5. Martensite Fraction versus Temperature for Various R_{ma} and R_{mb}

A simpler and more efficient way to accomplish the minor hysteresis loops is developed by changing R_{ma} and R_{mb} according to the Martensite fraction (R_m) of the SMA wire at the switching point. If the switching direction is from cooling to heating, the phase transformation model with $R_{ma} = R_m$ and $R_{mb} = 0$ represents the minor hysteresis loop to be switched to. While if the switching is from heating to cooling, $R_{ma} = 1 - R_m$ and $R_{mb} = R_m$ characterises the minor hysteresis loop to be switched to. In this manner, the SMA wire is no longer restricted to start on the major curve and the switching computation is easy to implement. Figure 3.6 illustrates the simulation of a SMA wire cycling within minor hysteresis loops with different starting phases obtained using the switching method described above.

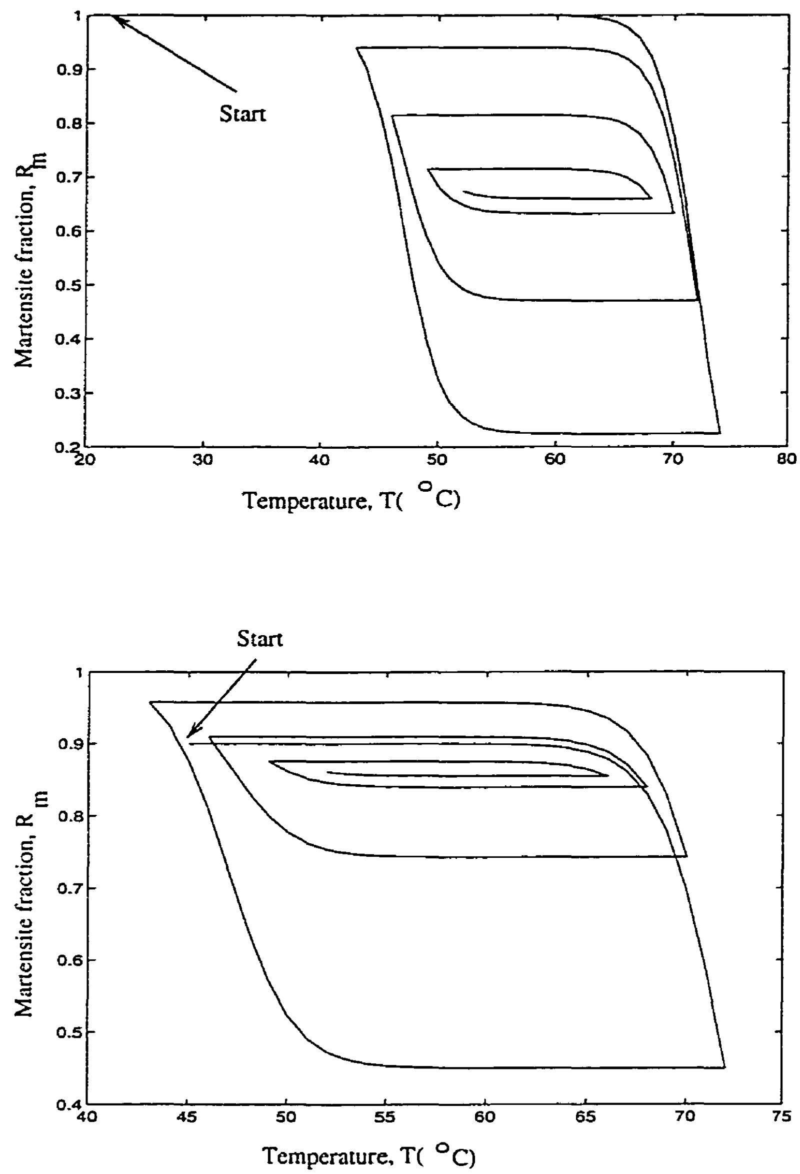

FIGURE 3.6. Cycling within Minor Hysteresis Loops

3.2. Stress Dependence of Phase Transformation. Equation (3.5) is derived under the assumption of zero load. However, the transformation temperatures A_s, A_f, M_s and M_f vary with the applied load [3]. The relation between the external stress and the transformation temperatures of a shape memory alloy can be approximated by:

$$\frac{d\sigma}{dT_r} = \frac{1}{c_m} \quad \textit{or equivalently} \quad T_r = c_m\sigma + T_0 \tag{3.8}$$

where

σ: external stress [MPa]

T_r: transformation temperature [°C]

T_0: transformation temperature under zero load [°C]

c_m: reciprocal of the stress rate (a constant)

Therefore, the formula on the Martensite fraction ratio including the effects of both stress and temperature can be expressed as:

$$R_m(T,\sigma) = \frac{R_{ma}}{1 + e^{k_m}(T - T_{0m} - c_m\sigma)} + R_{mb} \tag{3.9}$$

where the value of k_m and T_{0m} should be adapted from equation (3.6) for the cooling process, or equation (3.7) for the heating process. The quantity $(T_{0m} + c_m\sigma)$ is known as the generalized transformation temperature.

4. Stress-Strain Relationships

4.1. Stress-Strain Characteristics of Each Phase. Since the SMA behaves elastically at Austenite as depicted in Figure 3.7 , the stress-strain relationship of the P-phase is modelled as:

$$\sigma_p = E_p\epsilon \tag{3.10}$$

where ϵ is the axial strain, σ_p denotes the stress in a SMA wire under complete Austenite, and E_p indicates the elasticity.

The Martensitic phase exhibits a more complex relationship as shown in Figure 3.8. With the parameters defined in the figure, this nonlinear behaviour can be

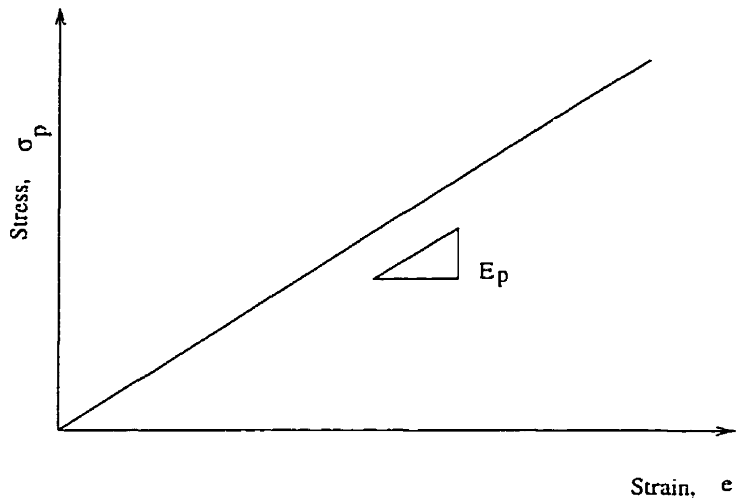

FIGURE 3.7. Stress-Strain Characteristics of Austenite

expressed as:

$$\sigma_m = \begin{cases} E_m\epsilon & 0 \le \epsilon < \epsilon_m^y \\ E_m\epsilon_m^y + E_t(\epsilon - \epsilon_m^y) & \epsilon_m^y \le \epsilon < \epsilon_m^d \\ E_m\epsilon_m^y + E_t(E_m\epsilon_m^d - E_m\epsilon_m^y) + E_d(\epsilon - E_m\epsilon_m^d) & \epsilon_m^d \le \epsilon \end{cases} \tag{3.11}$$

where σ_m is the stress in a SMA wire composed of Martensite alone.

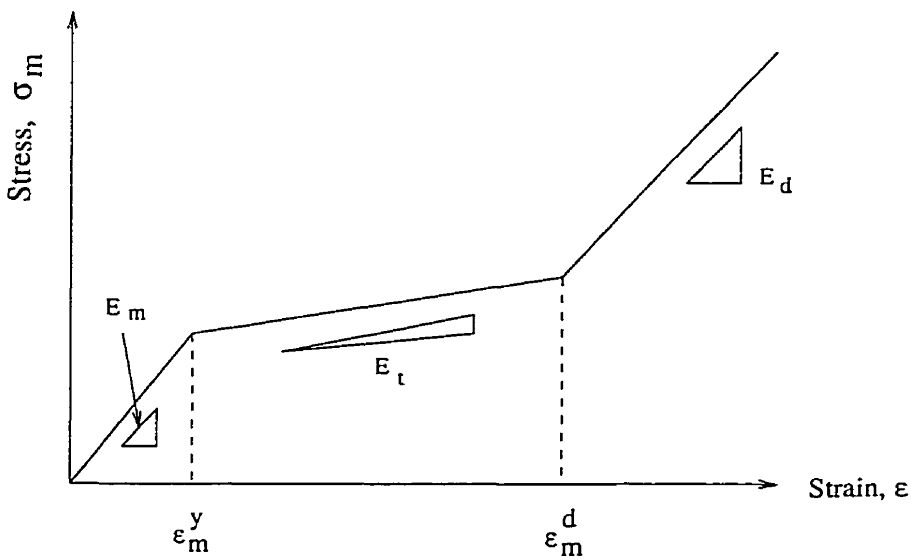

FIGURE 3.8. Stress-Strain Characteristics of Martensite

4.2. Overall Stress-Strain Relationship. The overall stress-strain relationship of the shape memory alloy is obtained using the variable sublayer assumption previously described. Since the total stress of a shape memory alloy is contributed by each sublayer proportionally to its phase fraction in the wire, this can be expressed as:

$$\sigma = R_p \sigma_p + R_m \sigma_m$$

where R_p and R_m are fractions of Austenite and Martensite respectively. Because the summation of R_p and R_m is always 1, the total stress can also be written as:

$$\sigma = (1 - R_m)\sigma_p + R_m \sigma_m \tag{3.12}$$

Combining equations (3.10), (3.11) and (3.12) yields an expression for the overall stress-strain relationship:

$$\sigma(\epsilon, R_m) = \begin{cases} R_m E_m \epsilon + (1 - R_m) E_p \epsilon & 0 \le \epsilon < \epsilon_m^y \\ R_m E_m \epsilon_m^y + R_m E_t(\epsilon - \epsilon_m^y) + (1 - R_m) E_p \epsilon & \epsilon_m^y \le \epsilon < \epsilon_m^d \\ R_m E_m \epsilon_m^y + E1 + E2 + (1 - R_m) E_p \epsilon & \epsilon_m^d \le \epsilon \end{cases} \tag{3.13}$$

where

$E1$: $R_m E_t (E_m \epsilon_m^d - E_m \epsilon_m^y)$

$E2$: $R_m E_d (\epsilon - E_m \epsilon_m^d)$

Sometimes strain may be the desired output. Equation (3.13) can be rewritten to express strain as a function of stress and the Martensite fraction:

$$\epsilon(\sigma, R_m) = \begin{cases} \frac{\sigma}{E_p - (E_p - E_m) R_m} & 0 \le \epsilon < \epsilon_m^y \\ \frac{\sigma + R_m (E_t - E_m) \epsilon_m^y}{E_p - (E_p - E_t) R_m} & \epsilon_m^y \le \epsilon < \epsilon_m^d \\ \frac{\sigma + R_m [(E_t - E_m)\epsilon_m^y + (E_d - E_t)\epsilon_m^d]}{E_p - (E_p - E_d) R_m} & \epsilon_m^d \le \epsilon \end{cases} \tag{3.14}$$

Figure 3.9 illustrates the strain versus Martensite fraction curves of a shape memory alloy while varying the load by 100 MPa steps from 200 MPa to 1000 MPa. The

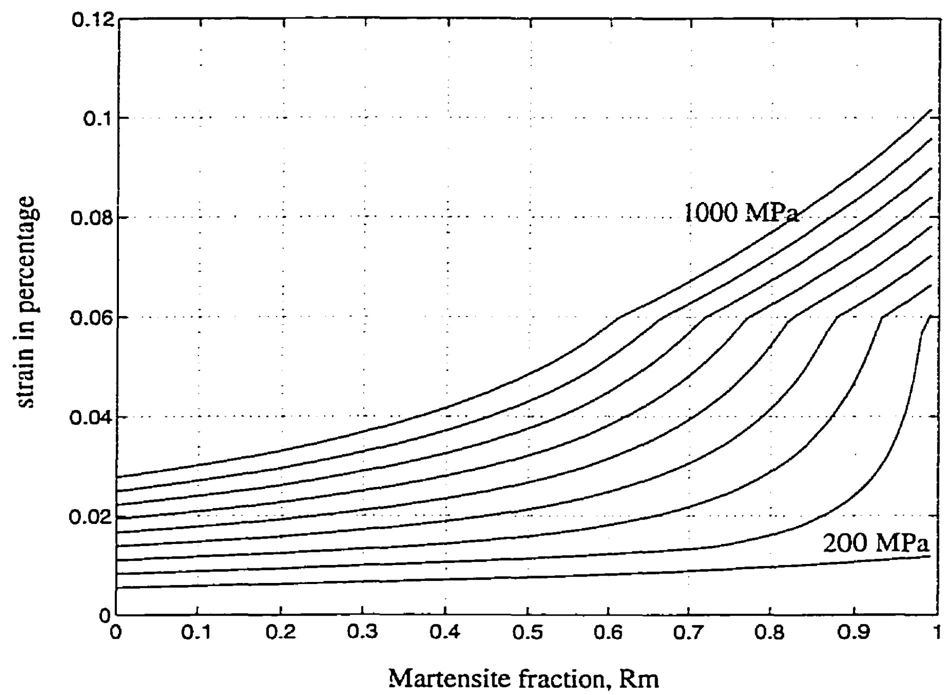

Parameter Values

$E_p = 35917$ MPa	$E_t = 826$ MPa	$E_d = 16800$ MPa
$E_m = 16800$ MPa	$e_m^y = 1.36\%$	$e_m^d = 5.96\%$

FIGURE 3.9. Strain versus Martensite Fraction for Various Loads

values of E_m, E_t, E_d, E_p, ϵ_m^y and ϵ_m^d chosen represent a type of NiTi SMA wire [**21**]. Note that the strain versus Martensite fraction relationship does not exhibit hysteresis, while the strain versus temperature relationship includes hysteresis due to the phase transformation. Figure 3.9 demonstrates the phase dependency of the mechanical characteristic of the shape memory alloy. As shown in the figure, when the stress applied to the wire is small (less than 200 MPa), the alloy falls into the tiny elastic region where $\epsilon < \epsilon_m^y$, hence the strain remains small regardless of the increment of the Martensite fraction. When the external stress increases such that $\epsilon > \epsilon_m^y$, the SMA yields at Martensite, therefore the strain significantly augments as the Martensite fraction increases in the wire. In practical applications, the strain of the SMA wire is never allowed to be greater than ϵ_m^d, otherwise the alloy will be damaged.

5. Experimental and Simulation Results

Experiments have been set up to identify the Young's modulus of one sample of NiTi shape memory alloy in Martensite and Austenite. The stress-strain curves are obtained when the SMA fiber is cold, or heated with constant step current input. Both experimental and simulation results are shown in Figure 3.10. The values of E_p, E_m, and E_t identified from experiments are 60000 MPa, 55784 MPa, and 15600 MPa respectively. E_t corresponds to the slope of the plastic region of the SMA's stress-strain curve of Martensite. The value of E_t of the NiTi shape memory alloy being tested is significantly larger than generally thought in theory, therefore the plastic region of the Martensite is not as flat.

Another characteristic typical to this NiTi wire is the spring effect. Ideally, a SMA in Martensite should retain most of the deformation when the external load is removed. However, it is observed in experiments that the SMA being tested recovers the deformation significantly even when the external stress is released in M-phase. In modelling, this is compensated by adding the spring effect to the plastic region of the Martensite. Consequently, when the external load is decreasing towards zero, the deformation of the alloy recovers a bit according to certain elasticity due to the spring effect. The spring constant identified from experiments is 37000 MPa for Martensite. In Austenite obviously, the spring constant coincides with the elasticity E_p. Therefore, the spring constant k at any phase mixture can be approximated by:

$$k = R_m k_m + (1 - R_m)E_p; \tag{3.15}$$

where k_m denotes the spring constant for Martensite.

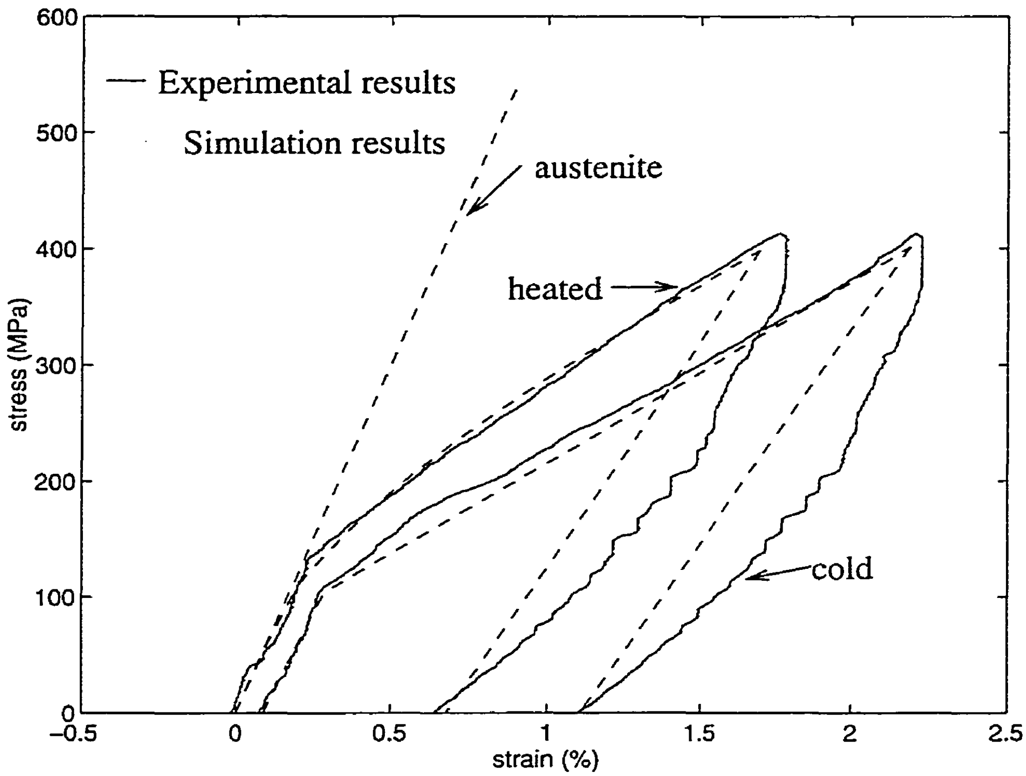

FIGURE 3.10. Stress-strain Relationships of SMA at different phases

CHAPTER 4

Modelling and Comparison of High Strain Shape Memory Alloy Actuators

A high strain shape memory alloy actuator consisting of a number of thin NiTi fibers woven in a counter rotating helical pattern around supporting disks was first proposed by Grant and Hayward [**6**]. The structure of the actuator is shown in Figure 4.1. "The disks are separated by preloading springs that keep the fibers under tension when relaxed. When the fibers are heated, they contract pulling the disks together. This structure can be viewed as a parallel mechanism used to accomplish highly efficient transformation between force and displacement. It overcomes the main mechanical drawback of shape memory alloys, that being of limited strain. Many of the conventional shape memory alloy actuators depend on mechanically amplifying the displacement either through the use of long straight fibers [**19, 20, 24**], or through the use of coils [**8, 3, 20**]. The proposed novel actuator achieves mechanical motion amplification which is more compact than a long straight length of fiber, and more efficient than using coils."

A substantial amount of work has been concerned with designing nonlinear controllers to perform on-line control to a pair of antagonist SMA actuators [**16**]. In this thesis, a computer software able to model various characteristics such as thermal, mechanical and geometric properties of this type of high strain actuator is first presented. This simulator is verified by experiments and further used to compare the performance of this type of SMA actuator with other actuator techniques given similar shape and actuation methods.

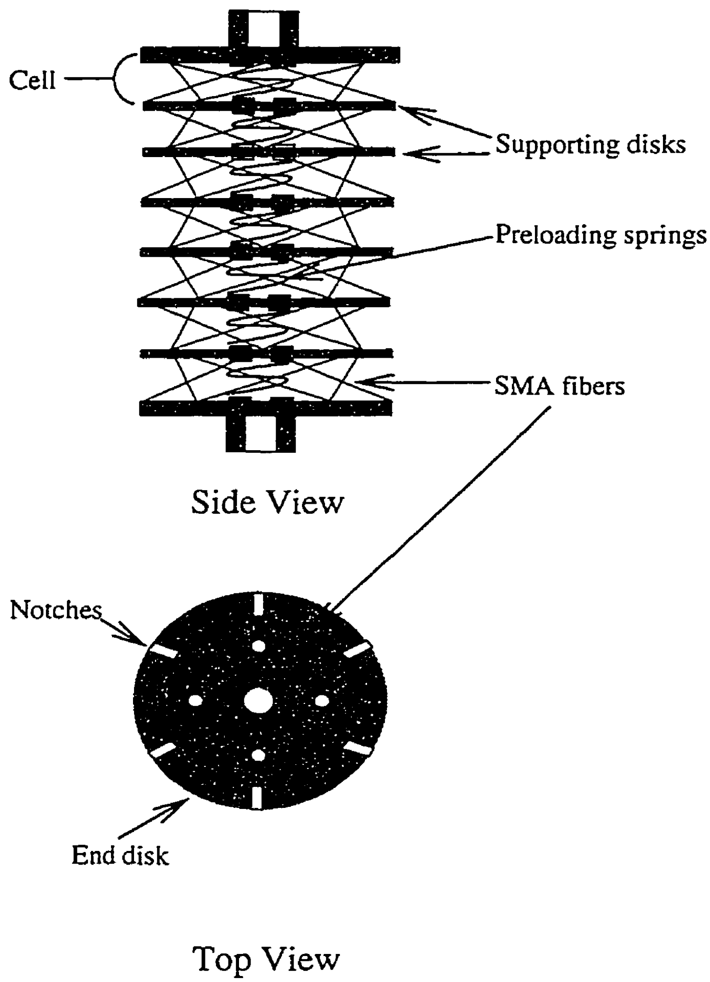

FIGURE 4.1. Shape Memory Alloy Actuator

1. Geometric Factor of the SMA Actuator

The geometric parameters involved in modelling the actuator are defined in Figure 4.2. For a detailed discussion about the weave pattern and construction of the actuator refer [**16**]. Let N_n be the number of notches around the disk, N_s be the number of disks in the actuator, and L_a be the actuator length. The following geometric relationships among design parameters can be derived:

$$d = \frac{L_a}{N_s - 1} \tag{4.1}$$

$$L = Dsin(\frac{\beta}{2}) \tag{4.2}$$

$$l = \sqrt{d^2 + L^2} = \frac{\sqrt{L_a^2 + (N_s - 1)^2 D^2 sin^2(\frac{\beta}{2})}}{N_s - 1} \tag{4.3}$$

$$\alpha = tan^{-1}\frac{d}{L} = tan^{-1}\frac{L_a}{(N_s - 1)Dsin(\frac{\beta}{2})} \tag{4.4}$$

L is the projection of the inter-disk fiber length l along the disk. As indicated in Figure 4.2, primitive d, L, and l form a right triangle in which the weave pitch angle α is defined.

The force-displacement characteristic of the SMA actuator is linked to the stress-strain relationship of the SMA fibers by a geometric factor. The kinematic amplification can be derived by first considering the simplified case consisting of two beams and one fiber as shown in the side view in Figure 4.2. As the fiber contracts, the tension in the fiber can be divided into an axial force F_a and a radial force F_r. Let t be the tension in the fiber, then

$$F_a = -t \cdot sin(\alpha). \tag{4.5}$$

Since the weave pattern of the actuator is always symmetric, all the radical components of the tension forces of the fibers cancel, leaving only a common axial stress force component $F_{actuator}$. If the number of notches around the disk is N_n, there are $2N_n$ fibers in one cell of the actuator. Therefore, the total axial force of the actuator can be expressed as:

$$F_{actuator} = -2N_n sin(\alpha) \cdot t \tag{4.6}$$

Clearly, $2N_n sin(\alpha)$ is the geometric factor which maps the kinematic gain of the SMA fibers to that of the actuator.

The displacement gain, defined as the change in stroke along the separating distance divided by the change in the fiber length is:

$$\frac{\Delta d}{\Delta l} = \frac{1}{sin(\alpha)} \tag{4.7}$$

Since the displacement gain is inversely proportional to the sine of the weave pitch angle, the smaller the weave pitch is constructed, the larger is the amplification of the absolute strain. Furthermore, the instantaneous displacement gain increases as the disks get closer together during the contraction. Comparing equation (4.7) with equation (4.5), it can be seen that the gain in stroke is obtained at the cost of the attenuation of the traction force. Therefore, the SMA actuator achieves a transformation between force and displacement according to the geometric factor which can be changed. In this manner, the actuator is no longer limited to the absolute percent strain of the fiber, while the force attenuation can be compensated for by using several fibers in parallel.

2. Force-Displacement Characteristic

Equation (4.6) written in detail is:

$$\begin{aligned} F_{actuator} &= -2N_n sin(\alpha) \cdot \sigma(\epsilon, R_m) \cdot s, \\ \epsilon = \frac{\Delta l}{l} &= \frac{\Delta d \cdot sin(\alpha)}{l} = \frac{\Delta L_a \cdot sin(\alpha)}{\sqrt{L_a^2 + (N_s - 1)^2 D^2 sin^2(\frac{\beta}{2})}} \end{aligned} \tag{4.8}$$

where s is the cross section area of the SMA fiber, ΔL_a denotes the stroke, and $\sigma(\epsilon, R_m)$ represents the phase dependent stress-strain function of the shape memory alloy defined by equation (3.13). Given the model of the SMA behaviour, the model of the actuator can be constructed based on equation (4.8) to predict the force-displacement characteristic, which resembles the shape of the stress-strain curves of the alloy.

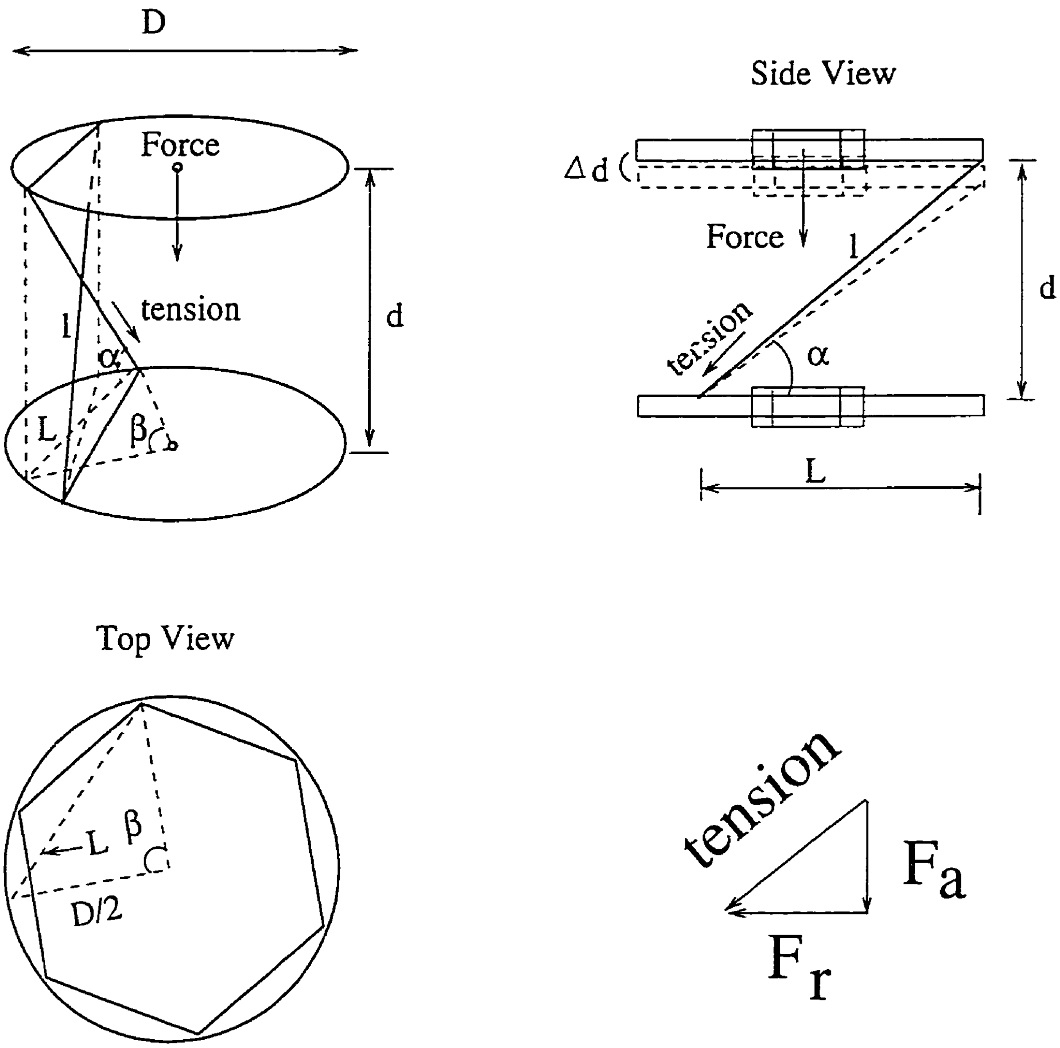

D - disk diameter

L - length of fiber along disk

β - offset angle between
succesive disks

l - length of fiber between disks

d - interdisk seperation

α - weave pitch angel

FIGURE 4.2. Variables Defined

In case the actuator displacement is the desired output, ΔL_a can be written as a function of the actuator force and other parameters:

$$\Delta L_a = -\frac{\sqrt{L_a^2 + (N_s - 1)^2 D^2 sin^2(\frac{\beta}{2})}}{sin(\alpha)} \cdot \epsilon(\sigma, R_m) \tag{4.9}$$

$$\sigma = \frac{t}{s} = \frac{F_{actuator}}{2N_n sin(\alpha) \cdot s}$$

where $\epsilon(\sigma, R_m)$ is the strain-stress function defined by equation (3.14).

The geometric parameters affect the dynamics of the SMA actuator in an inter-related fashion. For example, the displacement gain and stroke of the actuator can be augmented by increasing the disk diameter D, the trade-off being its size. The strength of the actuator can be intensified by using more fibers, or by using fibers with larger diameters. However, the former strategy raises the fiber interference, while the later one reduces the response time of the actuator. For an engineering application, an acceptable tradeoff must be chosen within set constraints so that the technical requirement is met. Figure 4.3 simulates the force-displacement curves of the SMA actuator in Martensite with one geometric parameter changing, the other parameters being held constant.

3. Design of Shape Memory Alloy Actuator

To design an actuator given the desired force, stroke, and dimension, equation (4.8) has to be solved for the design variables, as a function of given parameters. For example, the number of notches written as a function of other parameters is:

$$N_n = \frac{F_{actuator}}{2sin(\alpha)\sigma\left(\frac{\Delta L_a sin(\alpha)}{\sqrt{L_a^2+(N_s-1)^2 D^2 sin^2(\frac{\beta}{2})}}, R_m\right) \cdot s} \tag{4.10}$$

Of course, the value of N_n obtained from equation (4.10) should be rounded off to an integer.

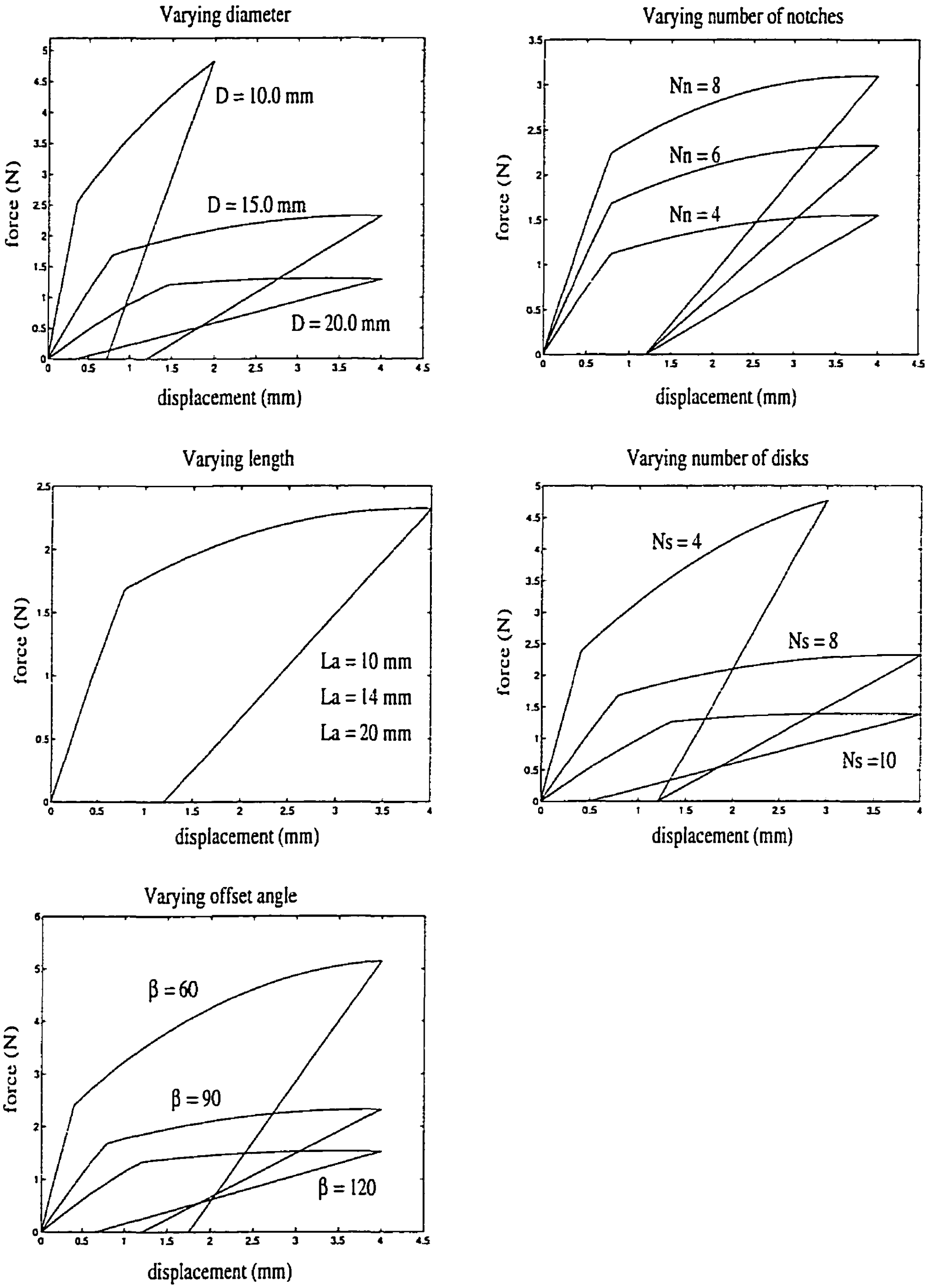

FIGURE 4.3. Force-displacement Curves With Changing Parameters

Solving other design parameters, such as D, L_a, or N_s as a function of given parameters involves higher order polynomial equations of which the closed-form solutions can not be obtained. Therefore, numerical methods including Newton and bisection algorithms for finding the roots of non-linear functions are used to determine these design variables. For example, Figure 4.4 illustrates how to select the length of the actuator according to different strength specifications given a desired stroke, diameter, number of notches and disks. In this particular case, under a certain maximum force, there are two lengths which can be selected for a given required force. Figure 4.5 describes how to select the number of disks under similar conditions.

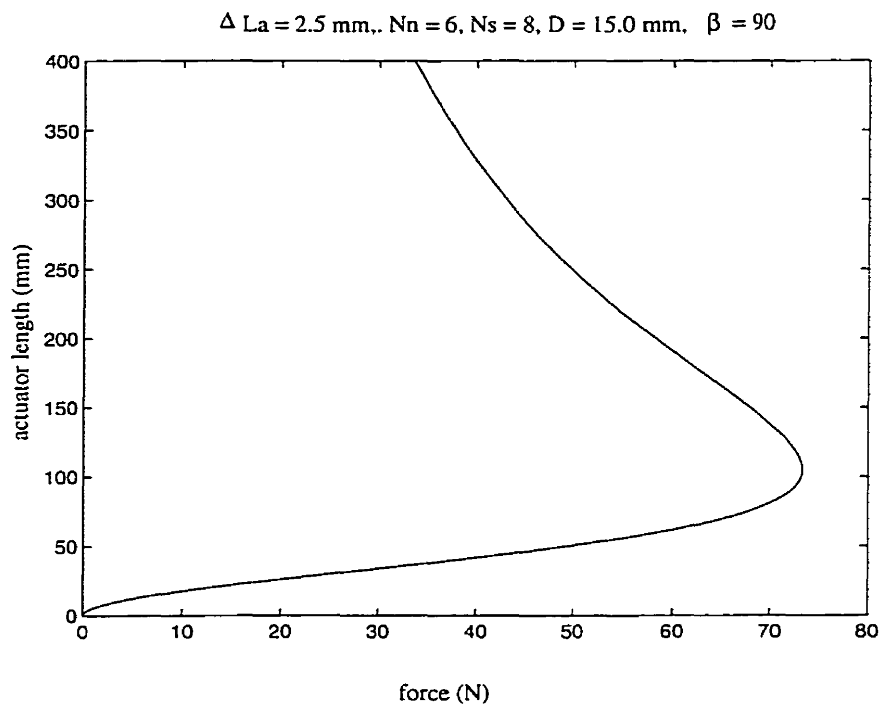

FIGURE 4.4. Designing the Length of a SMA Actuator

The modelling software can display relationships between any design variables. Of course, it is only convenient to plot relationship between two and sometimes three design variables. Due to its generality, the modelling software could be used by nonlinear search techniques in order to automate the design process.

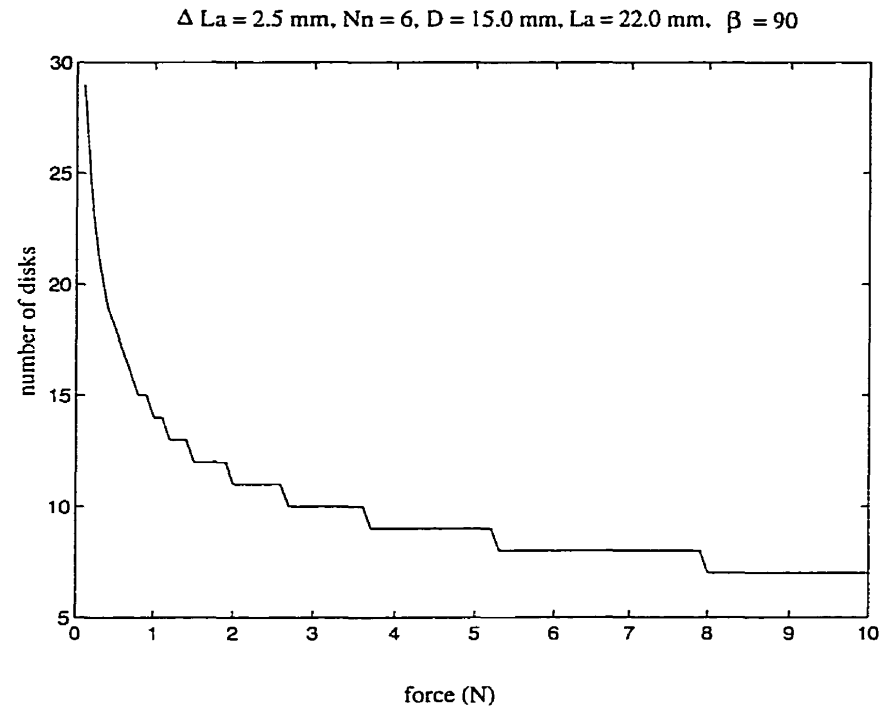

FIGURE 4.5. Designing the Number of Disks

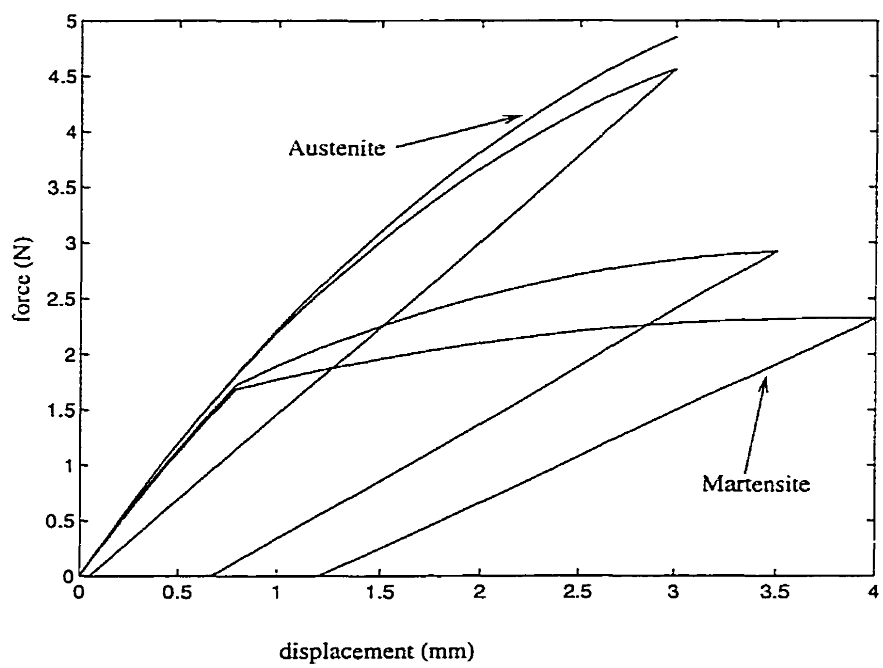

FIGURE 4.6. Force-displacement Curves of the Prototype Actuator

4. Experimental and Simulation Results

The prototype described in [6] implements only one among many possible configurations of the SMA actuator's geometry. 100 μm diameter SMA fibers were chosen for the actuator prototype which was designed to have a desired stroke of 2.5 mm. The actuator consists of 8 disks with 6 notches around each disk. The initial spacing of the disks was set at 2 mm. The actuator constructed is 6 grams in weight and fits inside a 17 mm diameter cylinder, 30 mm in length. The maximum pulling force is about 4 N. The simulation of the force-displacement relationship of this specific actuator is shown in Figure 4.6. As indicated from the simulation result, the force generated by the actuator in Austenite while recovering a stroke of 2.5 mm is about 4 N, which is consistent with the experimental result.

The fibers used in the actuator only exhibit one way shape memory effect. Therefore, two SMA actuators are arranged in an antagonistic fashion during experiments so that individual actuators will be forced to return to their original length when cooled. The antagonist actuator, being in the cold Martensite phase, produces a bias force which is accounted for in the model. The top view of the testbed is shown in Figure 4.7.

The experimental time domain open loop response to a set of step current input applied to the actuator was obtained by D. Grant [6] and the results are shown in Figure 4.8. The left side of Figure 4.8 shows the results of heating one of the actuator with a 50 ms pulse while varying the current amplitude by .3 A steps from 4.2 A to 7.8 A, and the right side of Figure 4.8 shows the results of heating the actuator with a constant current amplitude while varying the duration of the pulse between 20 ms and 65 ms. Note that the current in an individual fiber is divided by a factor of twelve since the actuator consists of twelve fibers in parallel. A constant time lag is observed at the beginning of the response curves, which accounts for the time spent to increase the temperature of the shape memory alloy to the Austenite starting temperature, A_s. The phase transition then begins and the fibers start to contract in an almost linear fashion.

The simulated trajectory curves shown in Figure 4.9 are obtained by modelling the response of the bias actuator under heating conditions described in the experiments. In order to fit the actuator model, the thermal constants defined by Equation (3.3) must be determined in order to give the temperature-current prediction of the SMA actuator. The thermal dissipation and capacitance extrapolated from the open loop response (Figure 4.8) are 2120.0 and 2.0 respectively. All the fitting parameters are listed in Appendix A.

In simulation, the bias actuator is pre-stretched by 6 mm as the maximum dynamic range. Upon heating, the SMA actuator recovers certain percentage of the stored strain according to the current-force-displacement relationship of the actuator previously established. If the fibers were heated to a temperature above the Austenite finish temperature, A_f, then the deformation will be completely recovered. Nevertheless, during experiments, the current is turned off before the temperature of the SMA fibers reach A_f so as to avoid overheating of the actuator. This indicates that the cooling processes undergo minor hysteresis loops. Therefore 1 , switching from major hysteresis loop to minor hysteresis loop must be considered when the current is turned off.

The simulation result gives good matches. It is easily noticed that the small ripples which are quite apparent on the experimental response are not present in the modelled response. This is easily explained by the fact that the load in the model does not include any inertial term, so second order dynamics are not modelled.

5. Comparison of High Strain Shape Memory Actuators

Having developed some confidence in the model, the performance of the actuation mechanism is compared to other existing technologies. In particular, the force-displacement and speed characteristics of a micro-solenoid electro-magnetic actuator

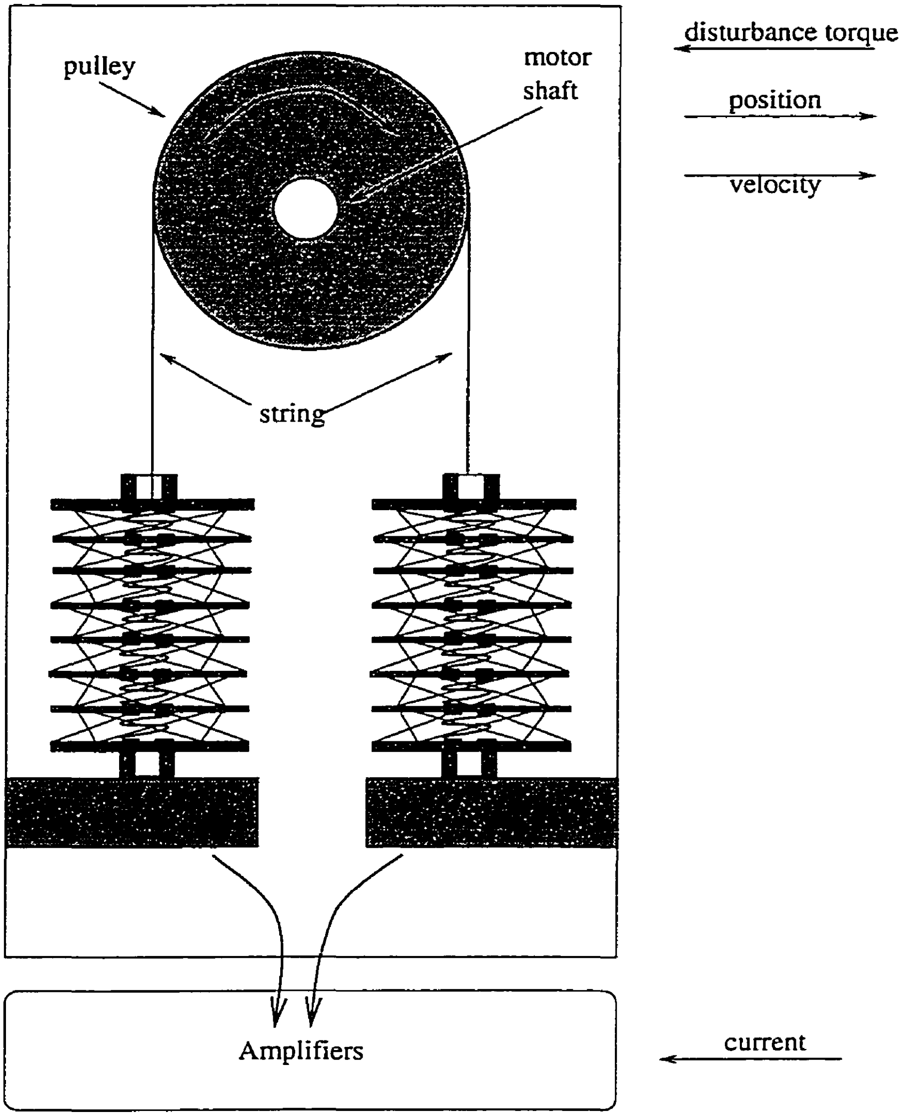

FIGURE 4.7. Top View of Testbed

and a muscle-size pneumatic actuator are compared to those of the SMA actuators with same dimensions.

5.1. A Micro-gripper Actuator. Ku et al. [25] developed a remotely controlled microgripper system for microsurgery application. A miniature electromagnetic solenoid actuator was chosen to drive the microgripper. It is an unidirectional device whose force depends on the position of its plunger. Its force-displacement curve

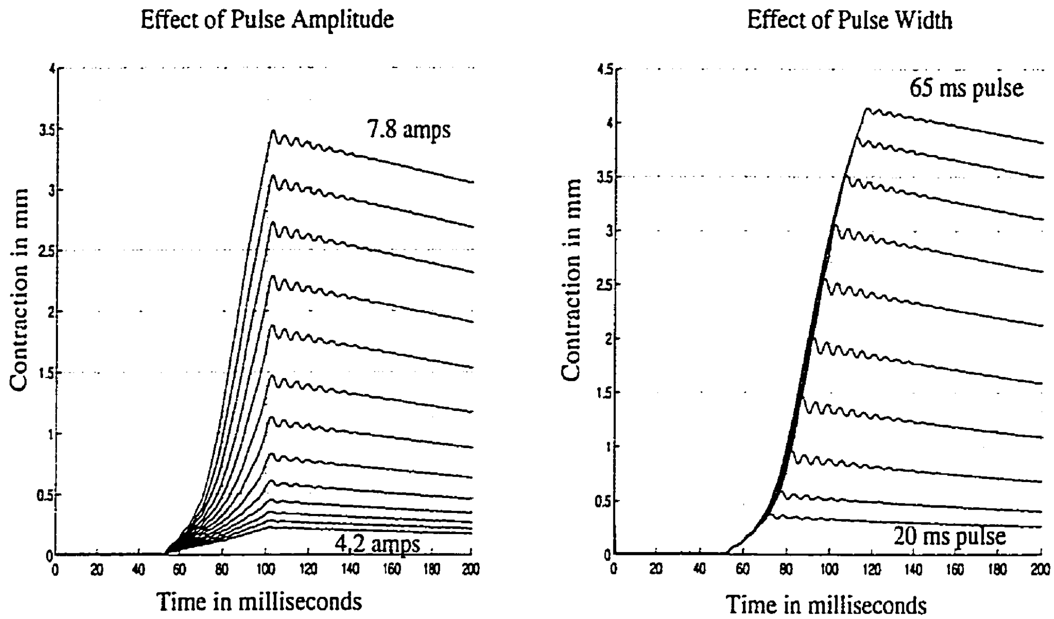

FIGURE 4.8. Open Loop Response

indicates that the maximum pulling force of the solenoid actuator at a displacement of 0.3 mm is less than 1 N.

We designed a SMA actuator to match the scale of the solenoid actuator used for the microgripper. The diameter and length of the solenoid actuator are estimated to be 6 mm and 13 mm respectively. Applying these constraints, two set of configurations were found. The corresponding force-displacement curves predicted are shown in Figure 4.10. In both cases, 100 μm diameter SMA fibers were chosen for the actuator.

The top of Figure 4.10 shows the force-displacement characteristic of an SMA actuator with 5 disks, 4 notches, and an offset angle of 90 degrees between successive disks. The pulling force that can be generated by the actuator with a stroke of 0.3 mm is greater than 5 N when the fibers are heated with the rated current, while the absolute strain of each fiber is less than 1%. One other configuration of the actuator with same length and diameter has 3 disks, 5 notches, and the offset angle is set to 108 degrees. The strength of the actuator is greater due to more fibers and a smaller displacement

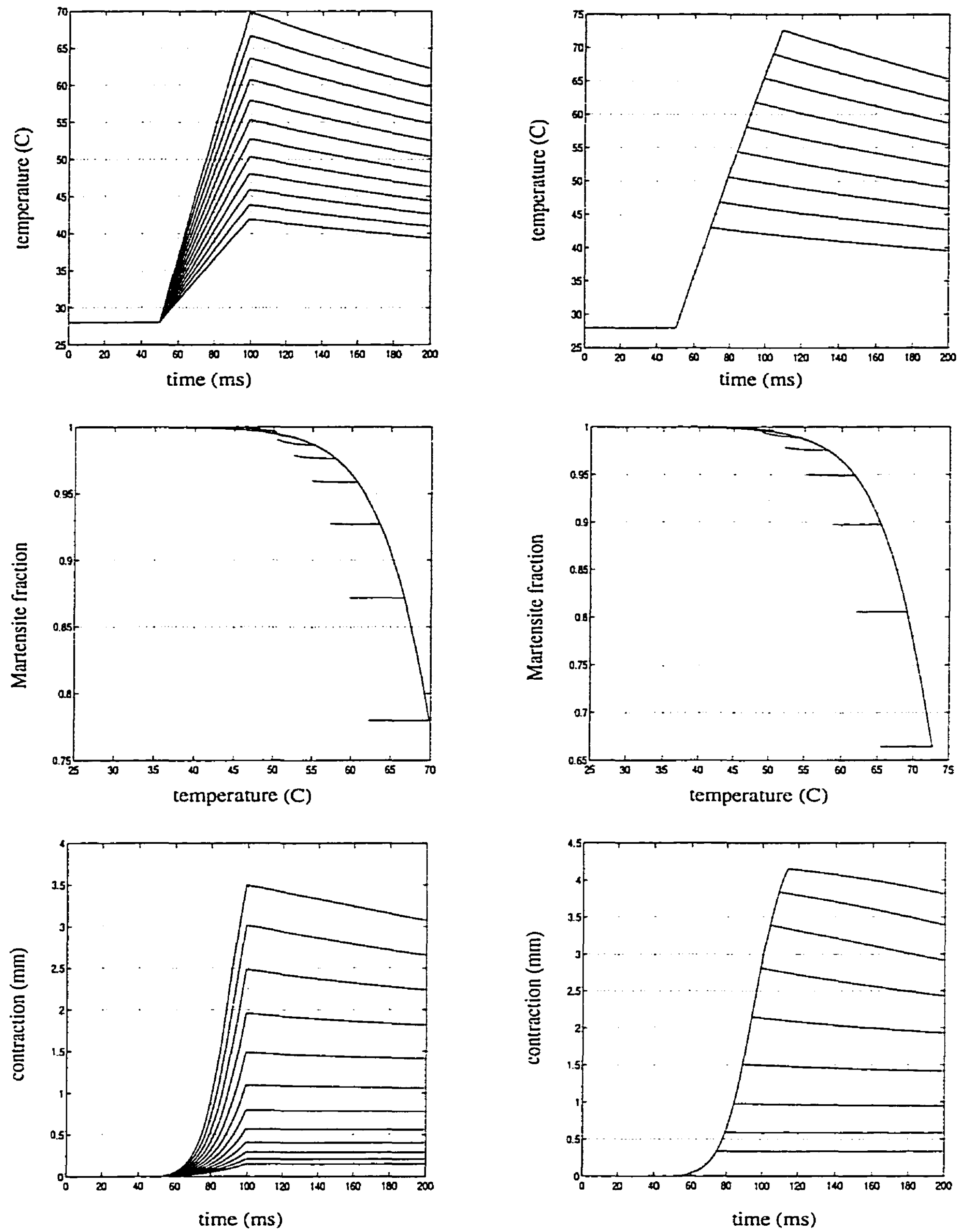

FIGURE 4.9. Simulation of the Open Loop Response

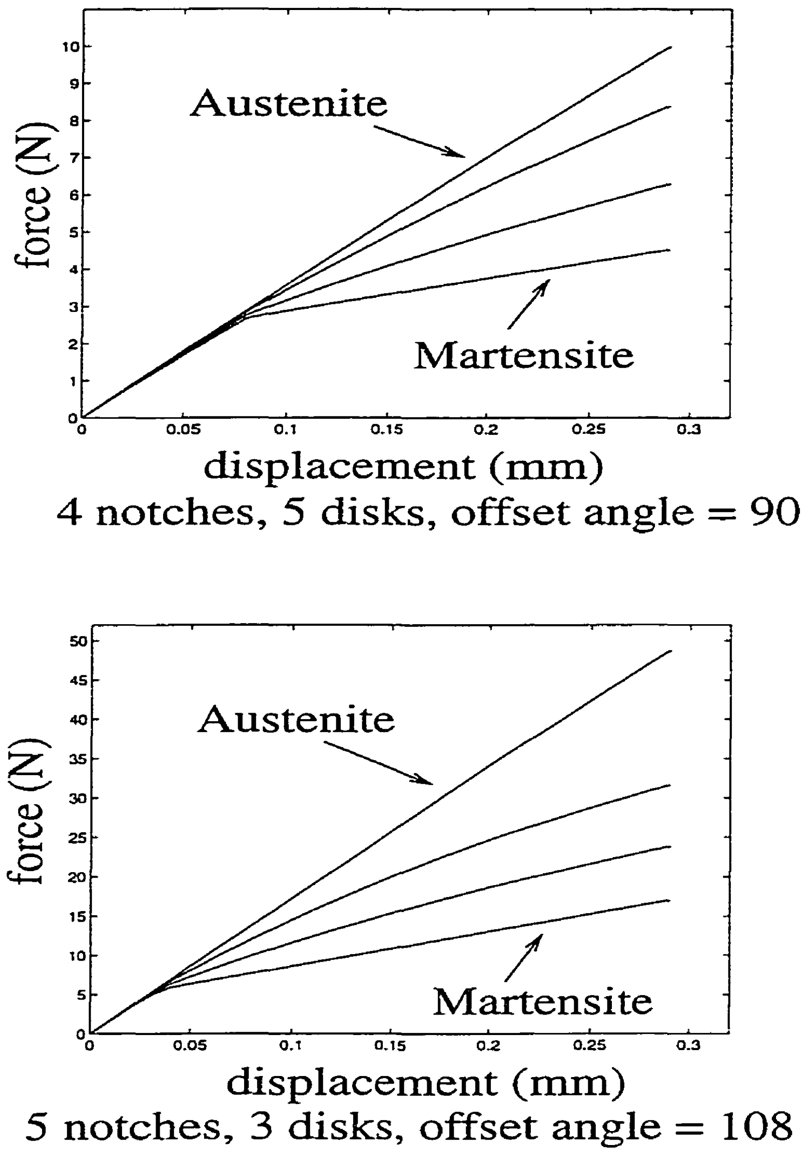

FIGURE 4.10. Force-displacement Curves of the Microgripper Actuator

gain. As a result, the fibers operate at an absolute strain of about 1.7% to achieve the 0.3 mm stroke, yielding a tension greater than 15 N.

The weight of the actuator at such scale would be about 2.5 grams. Clearly, it is much more powerful than the solenoid actuator with same size. In ambient air, the rise time would be about 30 ms. Bathed in a fluid, an order of magnitude of improvement would be expected.

5.2. An Artificial Muscle Actuator. The McKibben artificial muscle pneumatic actuator reported by Chou et al [**26**] consists of an internal bladder surrounded by a braided mesh shell. When the internal bladder is pressurized, the actuator shortens and produces tension if it is coupled to a mechanical load. The Bridestone McKibben actuator tested in [**26**] is 147 mm in length and 15 mm in diameter. The tension indicated from the experimental result at 4 bar pressure and 25 mm displacement is about 50 N. The maximum tension reported for this type of actuator is 260 N.

For the same length and diameter specified above, a SMA actuator could have 24 notches (48 fibers in parallel), 35 disks, and an offset angle of 90 degrees. The simulation of the force-displacement curves of the actuators using 100 μm and 200 μm diameter SMA fibers respectively are shown in Figure 4.11. The displacement gain is 3.4. The fibers in both actuators operate at 2% absolute strain to have a 25 mm stroke. The maximum tension of the actuator using 100 μm and 200 μm diameter SMA fibers are 38 N and 150 N respectively, with rated heating current. The weight of an actuator is about 16 to 20 grams. Using 200 μm diameter fibers results in a much stronger actuator, but suffering from an increased response time. We would expect the rise time of an actuator with the thicker fibers to be 60 ms. The Bridgestone actuator chosen from [**26**] for comparison yields the highest tension and stiffness intensities among all the pneumatic actuators reported in that paper. The maximum tensions for the McKibben actuators using nylon shell and fiberglass shell are 110 N and 56 N respectively. SMA actuators for a same size package would yield more strength than any of these designs. They also would be much simpler to manufacture and would not require servo valves. Experiments with smaller actuators using 100 μm fibers (fiber diameter is the dominating factor) indicate much wider dynamic range and speed ranges.

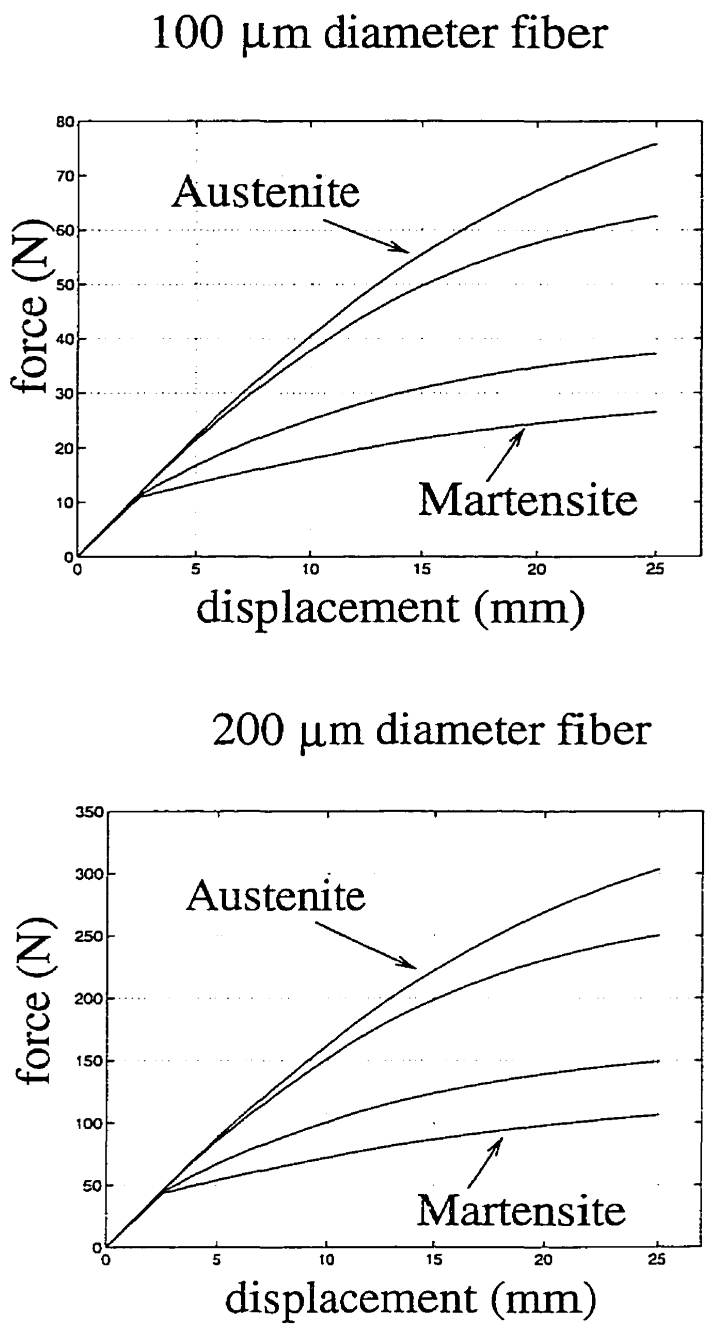

FIGURE 4.11. Force-displacement Curves of the Muscle Actuator

CHAPTER 5

Shape Memory Alloy Bending Actuator

There is a continuous demand for stronger, better, and smaller actuators possibly having several degrees of freedom. Actuators with bending feature, for example, can be used in a myriad of applications. In medical surgery, one of the needs is to insert a small tool in a narrow path of complicated nature. The smaller and more flexible the instrument is, the less pain and damage it will cause to the patient. In addition, its operation has to be accurate. To meet such challenges, research in the design of miniature active endoscopes has attracted much attention [**11, 12**]. Conventional endoscopes are mostly stiff in construction, with limited degree of freedom. Significant improvement will be possible if the stem of the endoscope can be adapted to the curvature path during the insertion. Shape memory alloy bending actuators provide a potential solution to similar problems.

1. Design of SMA Bending Actuator

Figure 5.1 illustrates a new concept of designing shape memory alloy bending actuator. Similar to the SMA tension actuator described in the previous chapter, the bending actuator also contains supporting disks with SMA fibers woven around. However, instead of using preloading springs to separate the disks, the bending actuator uses a hard rubber tube to connect the disks together. The rubber tube is able to bend when subject to a torque load and returns to its original shape as soon as the torque is released.

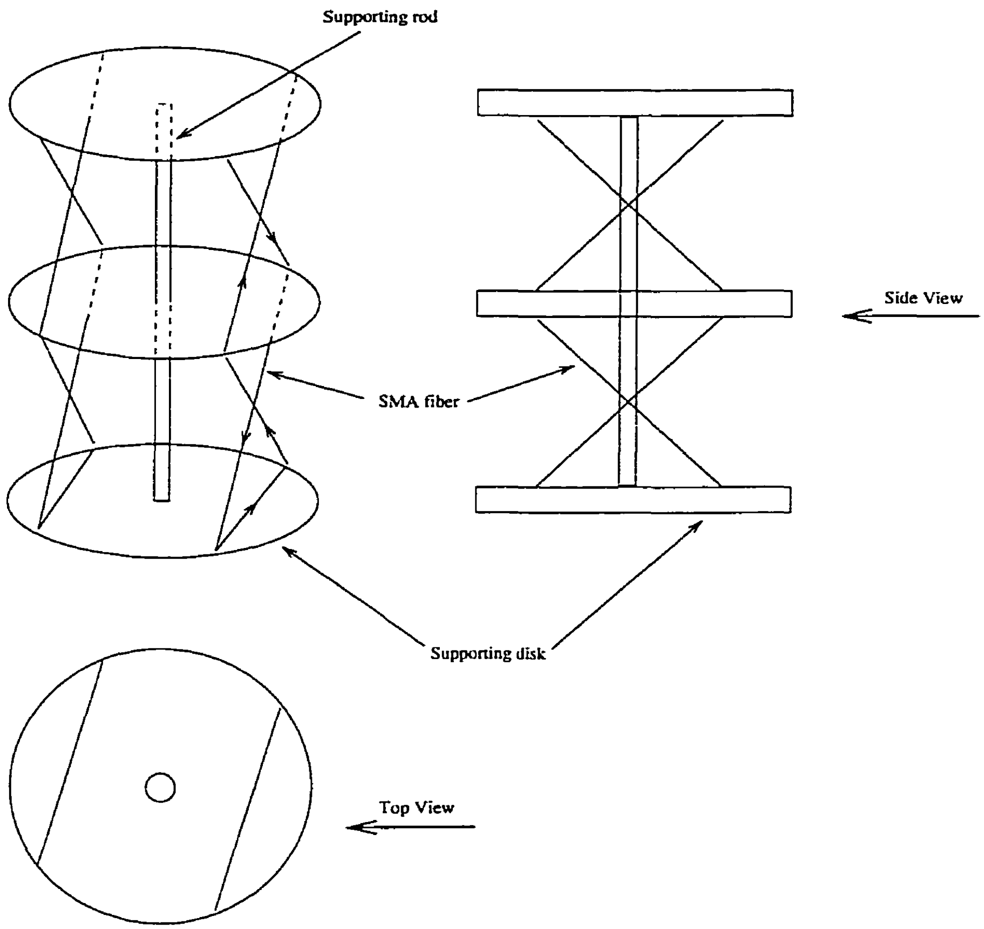

FIGURE 5.1. Simplified Structure of SMA Bending Actuator

The weave pattern of the SMA fibers is designed to ensure mirror symmetry. Therefore, fibers in the bending actuator always come in pairs. In Figure 5.1, the weaving of a single SMA wire is indicated by the arrows drawn along the fiber. When both fibers contract, the disks would be pulled together as in the tension case. However, if only one fiber is allowed to contract, the actuator bends as depicted in Figure 5.2. Clearly, the actuator constructed with one pair of SMA fibers has only two degree of freedoms. The direction of bending can be controlled by activating one of the SMA fibers selectively. In practice, the actuator can be constructed using

2 pairs of SMA fibers to achieve 4 degree of freedoms, or 3 pairs of SMA fibers to achieve 6 degree of freedoms. Figure 5.3 shows the top view of such design..

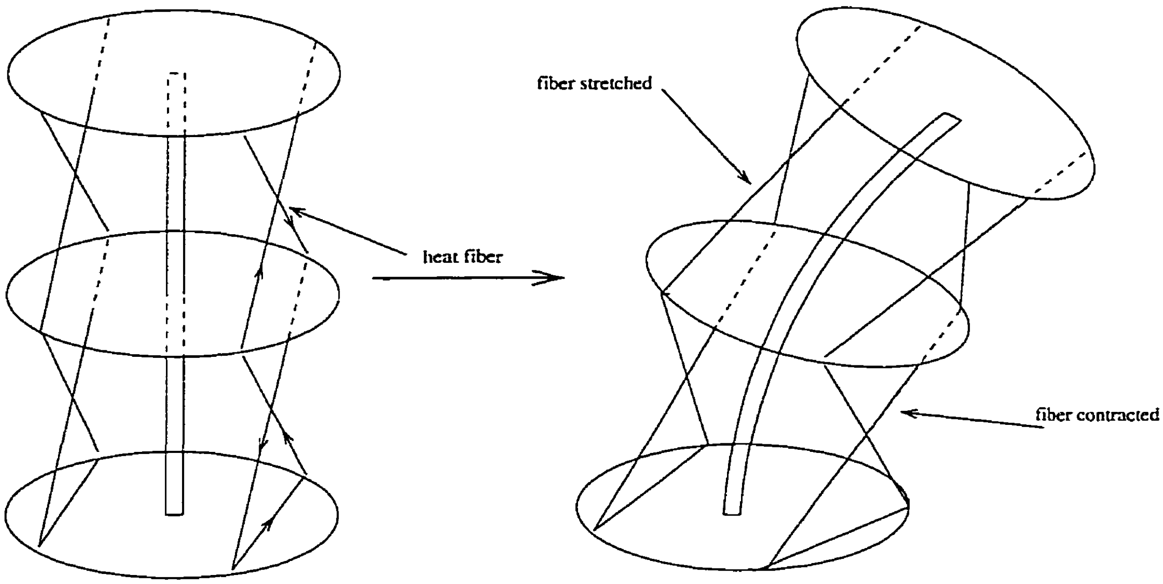

FIGURE 5.2. Bending of the Actuator

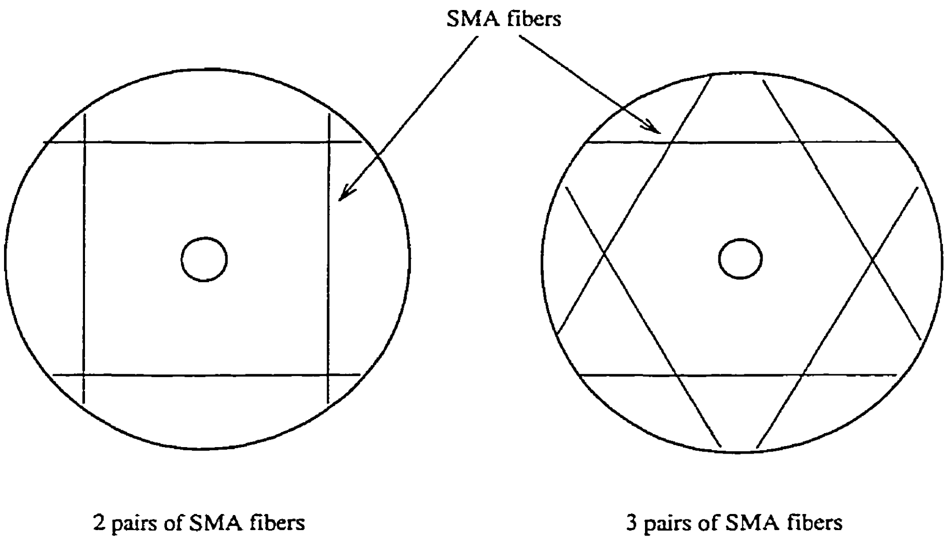

FIGURE 5.3. Top View of SMA Bending Actuator With High Degree of Freedom

2. Modelling of SMA Bending Actuator

To establish a dynamic model of the shape memory alloy bending actuator, the torque-angle relationship characterising the bending dynamics should be developed based on the stress-strain relationship of the SMA fiber and the geometry of the actuator. This, however, can't be easily achieved simply by using a geometric factor, as in the tension case. A bending actuator is not unidirectional, therefore when it bends, the active SMA fibers contract, while the inactive ones may stretch or remain undeformed. Depending on where the inactive SMA fibers locate relative to the active ones, their dynamic strains can be different from each other. In order to compute the overall strain energy distribution among the fibers, a general solution is obtained by tracking the intersections of the fibers and disks as the actuator bends. If the positions of those intersections (notches) can be determined as a function of the bending angle and the actuator geometry with respect to a reference coordinate, the absolute strain in each fiber can be uniquely determined during the bending.

The selection of a coordinate system is shown in (I) of Figure 5.4. The center of the bottom disk which is stationary during bending is chosen as the origin of the coordinate system. The bottom disk is in the X-Z plane, and the normal of the bottom disk is on the Y axis. Axes X, Y and Z form a right-hand system. The bending axis of the actuator may have an angle ψ from 0 to 360 degrees with respect to the reference coordinate (X axis), while the bending angle θ is defined as the angle of rotation of the disk normal around the bending axis, counter-clockwise rotation being positive.

Consider a nominal coordinate and bending axis orientation as shown in (III) of Figure 5.4. The bending axis coincides with the Z axis such that the track of the disk centers falls into the X-Y plane. To determine the geometric transformation of all the disk points, the position of each disk center after bending should first be determined. The coordinates of other points on a disk can then be calculated following the rules of 3D transformation [**27**]. In (II) of Figure 5.4, let O be the center of the fixed

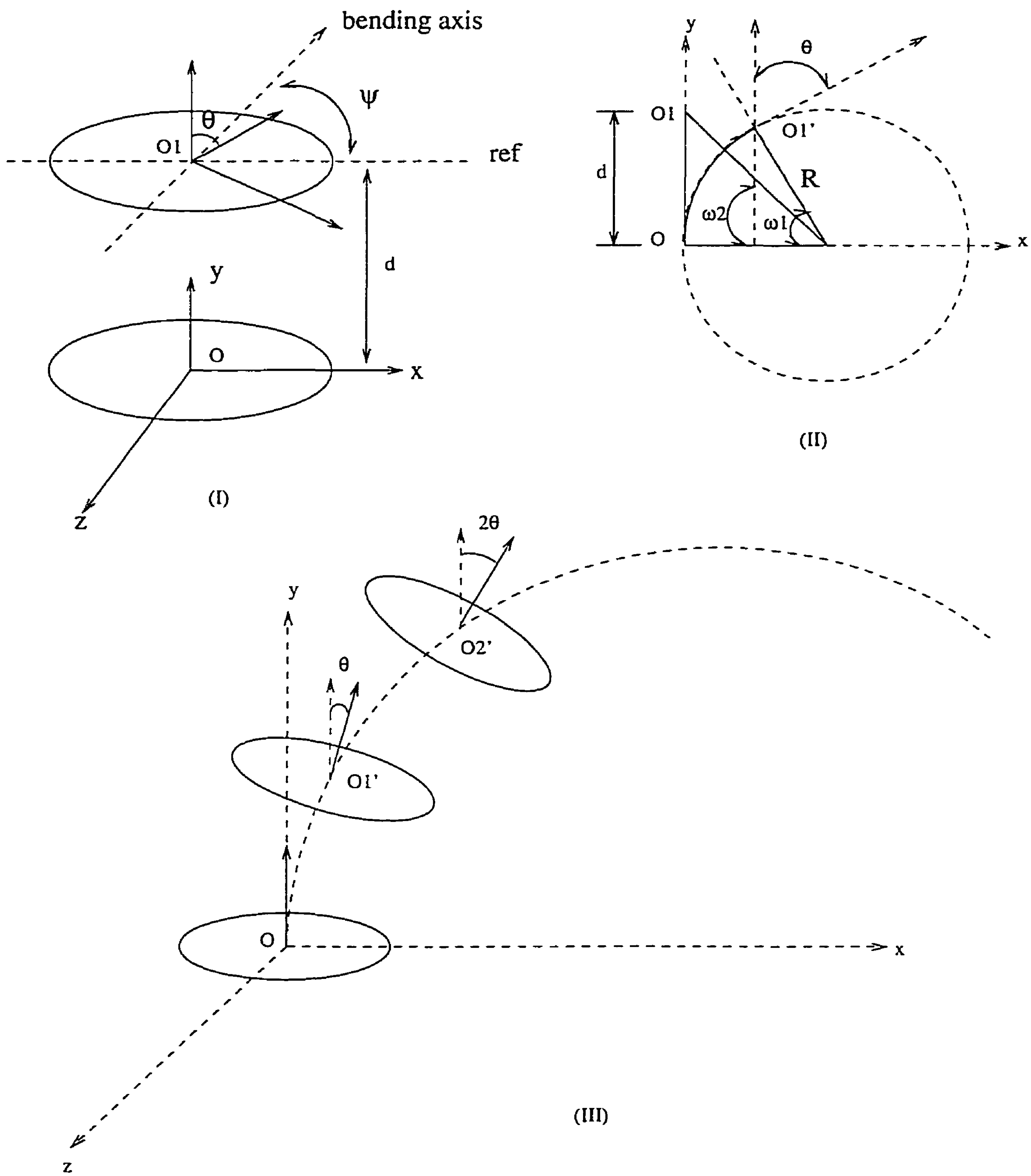

FIGURE 5.4. Geometric Transformation

stationary disk and O_1 be the center of the next successive disk separated with a distance of d. After bending θ degree, O_1 moved to the position of O_1' which is on a circle of radius R. Let ω_1 and ω_2 be defined as in (II) of Figure 5.4, then

$$\theta = \omega_1 \tag{5.1}$$

$$R = \frac{d}{\theta} \tag{5.2}$$

$$d = R \cdot tg\omega_2 = R \cdot \omega_1 \tag{5.3}$$

Therefore, the x and y coordinates of the center O_1' are:

$$x = R - R \cdot cos\theta = \frac{d(1 - cos\theta)}{\theta} \tag{5.4}$$

$$y = R \cdot sin\theta = \frac{d \cdot sin\theta}{\theta} \tag{5.5}$$

With the above information available, the transformation matrix to transform any points on disk O_1 due to bending can be formed as follows:

(i) Translate O_1' to the origin:

$$T(-x, -y, 0) = \begin{bmatrix} 1 & 0 & 0 & -x \\ 0 & 1 & 0 & -y \\ 0 & 0 & 1 & 0 \\ 0 & 0 & 0 & 1 \end{bmatrix} \tag{5.6}$$

where x and y are the coordinates of O_1'.

(ii) Rotate about the Z axis:

$$R_z(\theta) = \begin{bmatrix} cos\theta & -sin\theta & 0 & 0 \\ sin\theta & cos\theta & 0 & 0 \\ 0 & 0 & 1 & 0 \\ 0 & 0 & 0 & 1 \end{bmatrix} \tag{5.7}$$

(iii) Translate O_1' back to (x, y, 0):

$$T(x,y,0) = \begin{bmatrix} 1 & 0 & 0 & x \\ 0 & 1 & 0 & y \\ 0 & 0 & 1 & 0 \\ 0 & 0 & 0 & 1 \end{bmatrix} \tag{5.8}$$

The overall transformation matrix is:

$$T = T(x,y,0) \cdot R_z(\theta) \cdot T(-x,-y,0) \tag{5.9}$$

If the bending axis is not situated on the Z axis as defined by default shown in (III) of Figure 5.4, it can be rotated about the Y axis so that it coincides with Z. After that, the overall transformation matrix T may be applied to calculate the position of any point on the disk after the actuator bends by θ degrees. A software package is developed to take disk centers and notches as input, and return the dynamic strain of each fiber when the SMA actuator bends θ degree around any arbitrary bending axis. Some simulation results using this software are shown in Figure 5.5.

A sample of this type of SMA bending actuator with 4 degrees of freedom was fabricated in the laboratory and showed good prospects. The sensor and control strategy are being investigated. These are left for future work.

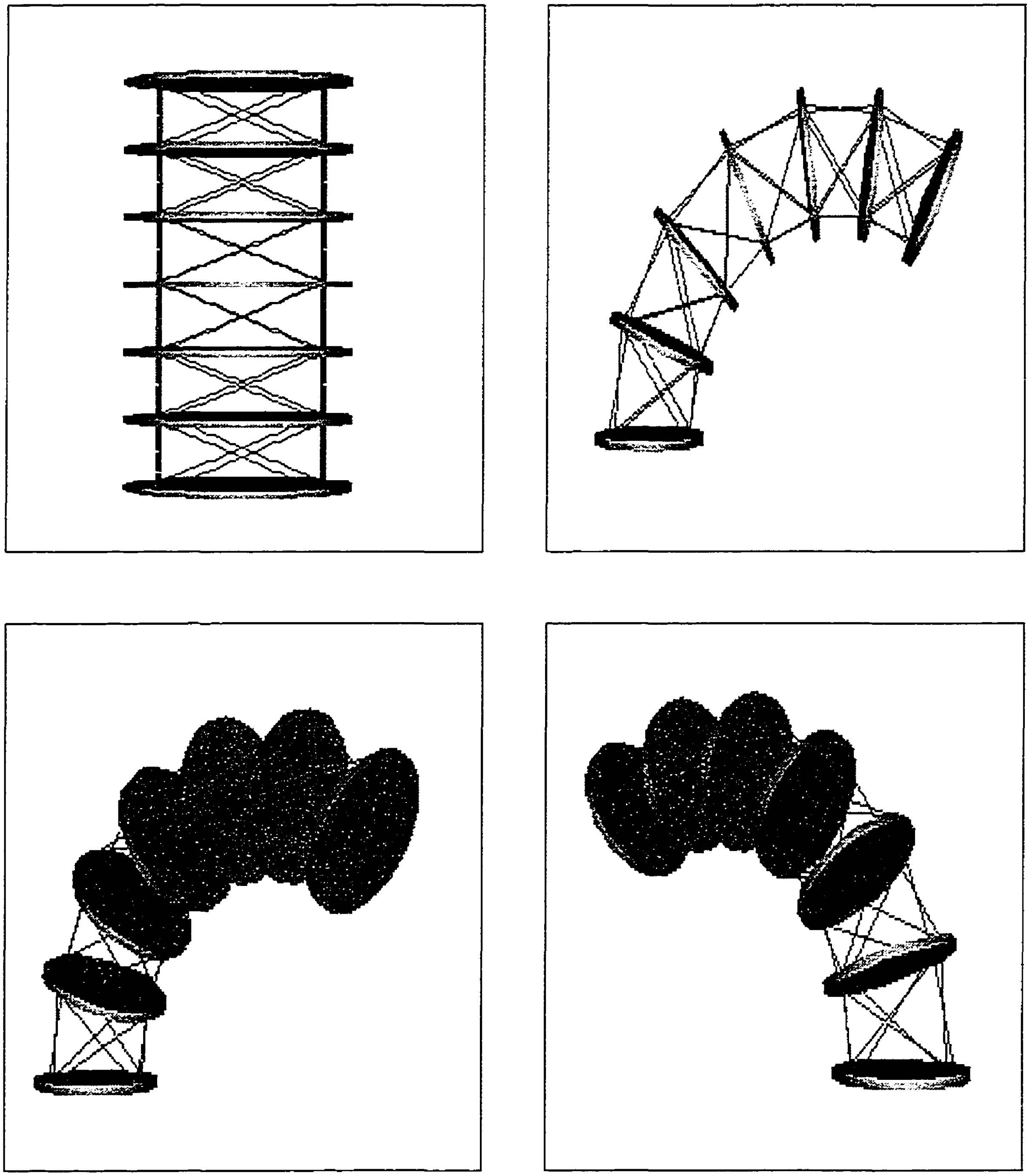

FIGURE 5.5. Graphical Simulation of Bending Actuator

CHAPTER 6

Conclusions

1. Conclusions

A software simulator for shape memory alloy actuator systems is constructed to predict the physical properties, geometric properties, and material properties of NiTi shape memory alloy high-strain actuators. Documentation of the software is included in Appendix B. This simulator can be used to predict the temperature-current relationship, phase-temperature relationship, and stress-strain relationship of a SMA fiber or actuator. It is also used to design geometries of a proposed SMA actuator under specifications such as force, stroke, size, and speed.

The Young's modulus of a NiTi shape memory alloy sample used in this research are identified from experiments for both Martensite and Austenite. The simulation results of the stress-strain relationship of the SMA sample are compared to those of the experiments and show good matches. The simulator is also applied to a prototype SMA actuator designed by Grant and Hayward. In particular, the simulation results of the current-force-displacement curves are compared to experimental results. The dynamics of a pair of antagonist SMA actuators constructed in the lab are well predicted, especially for the rising part of step responses.

The performance of such an actuator is compared with that of a miniature solenoid actuator and a pneumatic muscle size actuator under similar dimensions.

The SMA actuator is superior to the solenoid actuator in power, weight and displacement range. The comparison of the SMA actuator with the Bridgestone artificial muscle indicates that shape memory alloy actuators can also be employed in larger structures.

In the last part of the thesis, a new concept of designing SMA bending actuator is presented. The structure of the bending actuator is similar to that of the SMA tension actuator. It is also direct drive and may have high degrees of freedom. A software simulator is developed to model the geometric transformation of the actuator during bending, and to calculate the absolute strain of each SMA fiber woven around the disks. Graphical display of simulation results is implemented using in-house software package.

2. Future Work

Much future work can be done to improve the precision of the model of the SMA properties generated by the software simulator. In this research, the thermal property (temperature-current relationship) of the shape memory alloy fiber is not directly calibrated, due to the difficulty of measuring the temperatures of thin SMA fibers. Instead, the dissipation (C) and capacitance (a) that determine the thermal behaviour are identified from experimental stress-strain-current curves. Theoretical calculations of C and a are also possible, but suffer from volatile thermal parameters (heat capacity, resistance of the SMA fiber) and the imprecise heat transfer coefficient. If the temperature-current relationship can be determined experimentally, C and a could be better estimated and therefore contribute to a more accurate dynamic model.

Another unreliable parameter used in constructing the stress-strain-current model of shape memory alloy fiber is the coefficient c_m that accounts for stress-induced Martensite. c_m is defined in equation (3.8) as $\frac{dT_r}{d\sigma}$. Again, the inconvenience of measuring the temperature of a SMA sample hampers from calibrating this parameter experimentally. The value of c_m used by the simulator is estimated based on available technical specifications with reference to existing literature [**3, 21**].

In modelling of the prototype high-strain SMA actuator, the effect of pre-loading springs that separate the disks is ignored. This simplification will least affect the dynamic properties of the actuator in Austenite since the traction force generated by the actuator is much larger than the pushing force generated by the springs. However, as the SMA fibers cool to Martensite, they are easier to be deformed, therefore the effect of the pre-loading springs becomes more evident. For a more precise dynamic model of the actuator properties, the work done by the springs should also be considered when deriving the actuator force-displacement relationship.

Currently, the simulator is used to analyse and design NiTi shape memory alloy actuators, as well as comparing the performance of such actuators to other existing technologies. The application of the simulator can also be extended to controller design. In Grant's research [**16**], control of the high-strain SMA actuator was accomplished via a two stage switching feedback law. Since the controller switches according to the sign of errors, limit cycles always exist as the output of the system. To eliminate limit cycles, the nonlinear controller must be able to switch before the output exceeds the set point. One candidate solution is to use a well calibrated dynamic model to predict the output of the system a few time steps in advance. If a potential overshoot is detected according to the prediction, the control input can be switched based on this information before an error occurs.

The research to design, model and control shape memory alloy bending actuator is just in its infancy and much is left as future work. The software simulator presented in the previous chapter is capable of computing the absolute strain of each SMA fiber in the actuator given the bending axis and angle. Further work needs to be done to establish the torque-angle relationship of the bending actuator and also to design an appropriate controller.

APPENDIX A

Properties of NiTi

The physical property parameters of the NiTi wires used in this research have two sources: the technical specification provided by the manufacturer [28], and the experimental estimation. In the following breakdown, those parameters that are not taken from [28] are marked with '*'.

- Diameter of the NiTi fiber - 0.1 μm
- Density - 6500 [kg/m^3]
- Specific heat - 553 [J/kg °C]
- Electrical linear resistivity - 118 [Ω/m]
- *Heat transfer coefficient - 59 [W/m^2 °C]
- Transformation temperatures:
  - $M_s = 72.0$ [°C]
  - $M_f = 62.0$ [°C]
  - $A_s = 87.5$ [°C]
  - $A_f = 97.5$ [°C]

- Stress-strain parameters:
  - $E_p = 60000.0$
  - $E_t = 15600.0$
  - $E_m = 55784.0$
  - $*E_d = 16800.0$
  - $\epsilon_m^y = 0.001829$
  - $*\epsilon_m^d = 0.0596$
- *Coefficient of stress induced Martensite (c_m): 0.01 - 0.1
- Weight of supporting disks:
  - Plastic: white - 0.25 [g], black - 0.3 [g]
  - Alumni: white - 0.63 [g], black - 0.37 [g]
  - Brass: 1.96 [g]
- *Thermal parameters: dissipation - 2120.0, capacitance - 2.0

APPENDIX B

Design Description of the Software Simulator

The software simulator introduced in this thesis was developed using C++ in order to take the advantage of the Object Orientated (OO) programming concept. Modelling of shape memory alloy actuators is especially suitable for OO programming because a NiTi fiber can be considered an object (a class) with many properties (class functions), while an actuator made of SMA fibers form another object which can be constructed by integrating the actuator geometry with the fiber properties. The Inheritance feature of C++ provided a convenient way to implement the above feature and generate more reusable codes. The whole program consists of three modules: SMA fiber, SMA tension actuator, and SMA bending actuator.

1. SMA Fiber

This module contains three sections:

- fiber.h This is the definition section which contains declaration of all the variables and classes.
- fiber.C This section is the entry of the module (*main()*). Class parameters must be initialized here before the class can be used to predict properties of a specific SMA fiber.

- fiber_fun.C This is the implementation section which implements the procedures and class functions defined in fiber.h.

There are four major classes in this module: sma_TP, sma_SS, sma_GP, and sma_MP. They are built to predict different aspects of the shape memory alloy properties.

(i) SMA Thermal Property Class - sma_TP

This class is designed to model the temperature-current relationship (*T_current*) and the phase-temperature relationship (*Rm_T_sigma* or *Rm_T_epsilon*) of SMA fibers as discussed in Chapter 3. The data of the class are parameters of a SMA fiber that have to be specified by a user. Appendix A gives a set of parameter values that have been used for this thesis. The class variables are initialized in the main() procedure following the declaration of an instance of the class. Function *Rm_T_sigma* and *Rm_T_epsilon* are quite straight forward to use. They have to take stress (sigma) or strain (epsilon) in the input due to the fact of the *Stress Induced Martensite*. An overview of the structure of this class is given in figure B.1.

(ii) SMA Stress-Strain Property class - sma_SS

This class is a child of the class sma_TP therefore it inherits all the private data and public functions of the SMA thermal property class (sma_TP). In addition, it adds several more functions to model the stress-strain relationship of a given SMA fiber. The stress-strain functions can be based on the Martensite fraction (*Strain_stress_Rm*, *Stress_strain_Rm*), or based on the temperature (*Strain_stress_T*, *Stress_strain_T*). Function *Plastic_strain_stress* (or *Plastic_stress_strain*) characterized the spring effect existing in common shape memory alloys. For a Martensite SMA fiber, ideally it should retain the deformation after the external stress is released. In reality, it actually recovers certain percentage of that deformation after the stress is gone. This behaviour is considered as the spring effect. Function *Plastic_strain_stress* returns the

Class sma_TP (Thermal Properties of the shape memory alloy fiber):

Private Data:

- Ms - Martensite starting temperature
- Mf - Martensite finishing temperature
- As - Austenite starting temperature
- Af - Austenite finishing temperature
- Rma, Rmb, T0m_c, k_mc, T0m_h, k_mh - constants that determine the phase transformation model
- c1, c2, a - constants that determine the Temperature-current curve
- Tinf - the ambient temperature

Public Member Functions:

- get_tc
- set_TP
- set_SS
- switching
- Rm_T_epsilon — RTBIS — FUNC_Rm — range / Rm_T_sigma
- Rm_T_sigma — T0m_km
- T_current — trapzd
- T_step
- T_cooling

FIGURE B.1. Thermal Property Class - sma_TP

actual strain of a Martensite fiber after the external stress is released. The input variables $s0$ and $e0$ of this function are the stress and strain values of the fiber at the time the stress dropped to 0. Figure B.2 provides the structure of the class as well as the calling tress of the public member functions.

(iii) SMA Geometric Property class - sma_GP

This class is a also a child of the class sma_TP. The objective of sma_GP is

Class sma_SS (Stress-Strain relationship of the sma fiber)

Private Data:

all the private data of sma_TP

Public Member Functions

all the public functions of sma_TP

Stress_strain_Rm — range

Strain_stress_Rm — range

Strain_stress_T — Rm_T_sigma
Strain_stress_T — Strain_stress_Rm

Stress_strain_T — rtbis — func — Rm_T_sigma

Plastic_stress_strain

Plastic_strain_stress

FIGURE B.2. Stress-Strain Property class - sma_SS

to determine the relationship between the length and cross-section of a SMA fiber when other parameters are given as specifications. Figure B.3 illustrates the structure of the class.

(iv) SMA Material Property class - sma_MP

The material property here refers to the Young's modulus parameters of a SMA fiber. When the geometry, force and displacement specification of the

Class sma_GP (Geometric Properties of SMA fiber)

Private Data

all the private data of class sma_TP

F - force generated by the fiber

dl - stroke of the fiber

Public Member Functions

set_GP

crosection_length
- Rm_T_epsilon
- range

length_crosection
- Rm_T_sigma
- range

FIGURE B.3. Geometric Property Class - sma_GP

fiber is given, the relationship of the Young's parameters is fixed. This class is built to reflect the characteristics of those parameters under such a condition.

2. SMA Tension Actuator

This module contains three sections:

- actuator.h - The definition section.

- actuator.C - The main and entry procedure.
- actuator_fun.C - The implementation section.

There are three classes defined in this module: actuator_base, actuator_FS, and actuator_GP. They can be used to predict the force-displacement relationship and the geometric relationship of the high strain shape memory alloy actuator introduced in Chapter 4.

(i) Shape Memory Alloy Actuator Base Class - actuator_base

This is a child class of sma_SS of the SMA fiber module. Clearly, it inherits all the functionalities for predicting SMA fiber properties. Furthermore, it calculates the geometric factor that maps the stress-strain relationship of the SMA fibers to the force-displacement relationship of the actuator, through the class function geo_factor(). The five in-line functions in this class are for changing the geometry, fore example, diameter, length, etc of the actuator. When these factors change, the geometric factor changes too. Function Alpha() returns the weave pitch angle, while function Pattn_fib_length() calculates the fiber length between two successive notches. Figure B.4 illustrates the structure of this class.

(ii) SMA Actuator Force Stroke Relationship Class - actuator_FS

This class is a child of the class actuator_base. It predicts the force-stroke relationship of a given SMA actuator through class functions Force_stroke and Stroke_force. Function Rm_T_force describes the phase-temperature relationship of the actuator, with consideration of the *Stress Induced Martensite.* Function Plastic_stroke_force is similar to functions Plastic_stress_strain and Plastic_strain_stress of the module SMA fiber. It models the spring effect of the actuator caused by SMA fibers. Function Strain_recover calculates the strain of the actuator that will be recovered upon heating, given a pre-stretch value

Class actuator_base (base for constructing the actuator model)

Private Data

all the private data of class sma_SS

Protected Data

D - actuator Diameter

beta - the offset angle of the actuator

la - actuator length

Nn - number of notches

Ns - number of stacks

Public Member Functions

Alpha	change_length	
Pattn_fib_length	change_Diameter	change_offset_angle
geo_factor —— Alpha	change_Notch_num	change_Stack_num

FIGURE B.4. Actuator Base Class - actuator_base

and the external force applied to the actuator. Function actuator_FS simply initializes the actuator parameters with given values. Figure B.5 depicts the structure of this class.

(iii) SMA Actuator Geometric Property Class - actuator_GP

This class is also a child of the class actuator_base. It can be used to design actuator geometries while the force, stroke and the other parameters are

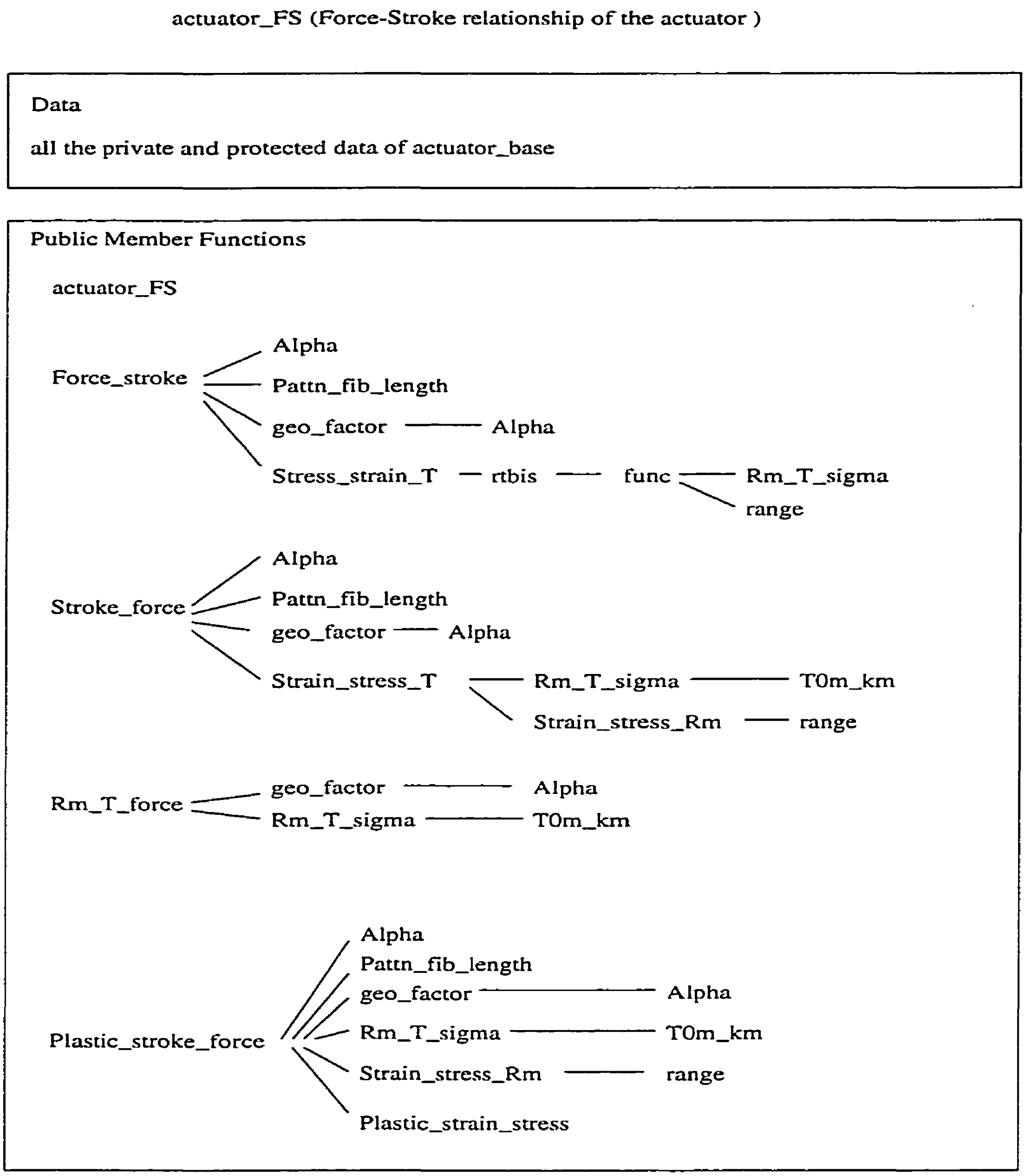

FIGURE B.5. Actuator Force-Stroke Property Class - actuator_FS

specified by users. Function Notch_force_stroke and Stack_force_stroke determine the number of notches and stacks (disks) to be used in an actuator so as to achieve the force and stroke specified under certain constrains. Function actuator_length and actuator_Diameter design the length and diameter of an actuator under similar conditions. Initialization of the private data of the class is done through function actuator_GP. Figure B.6 shows the structure of this class.

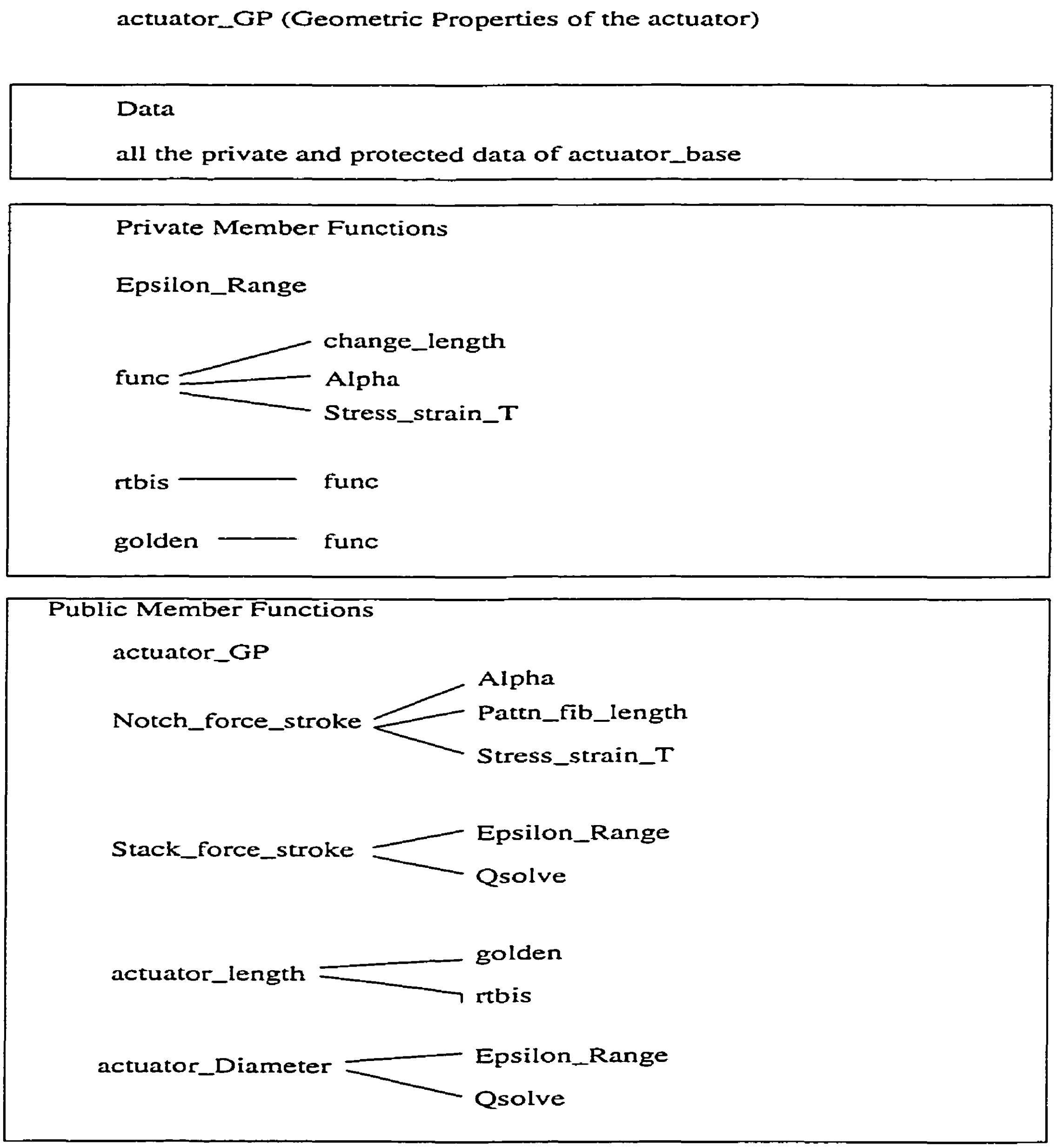

FIGURE B.6. Actuator Geometric Property Class - actuator_GP

3. SMA Bending Actuator

This module contains three sections:

- bend.h - The definition section.
- bend.C - The main and entry procedure.
- bend_fun.C - The implementation section.

The two major classes in this module are bend_geometry and list. The data of the class bend_geometry are Edges og (original) and td (transformed). The class functions perform the required geometric transformation according to the given bending angle and bending axis, and keep the result in Edge td. Class list describes a link list object whose class functions can add new elements to the beginning or end of the link list. The list class records the length of the link list, the head and tail address of the list into its private data and keep them updated. The structure of the two classes are illustrated in Figure B.7 and Figure B.8.

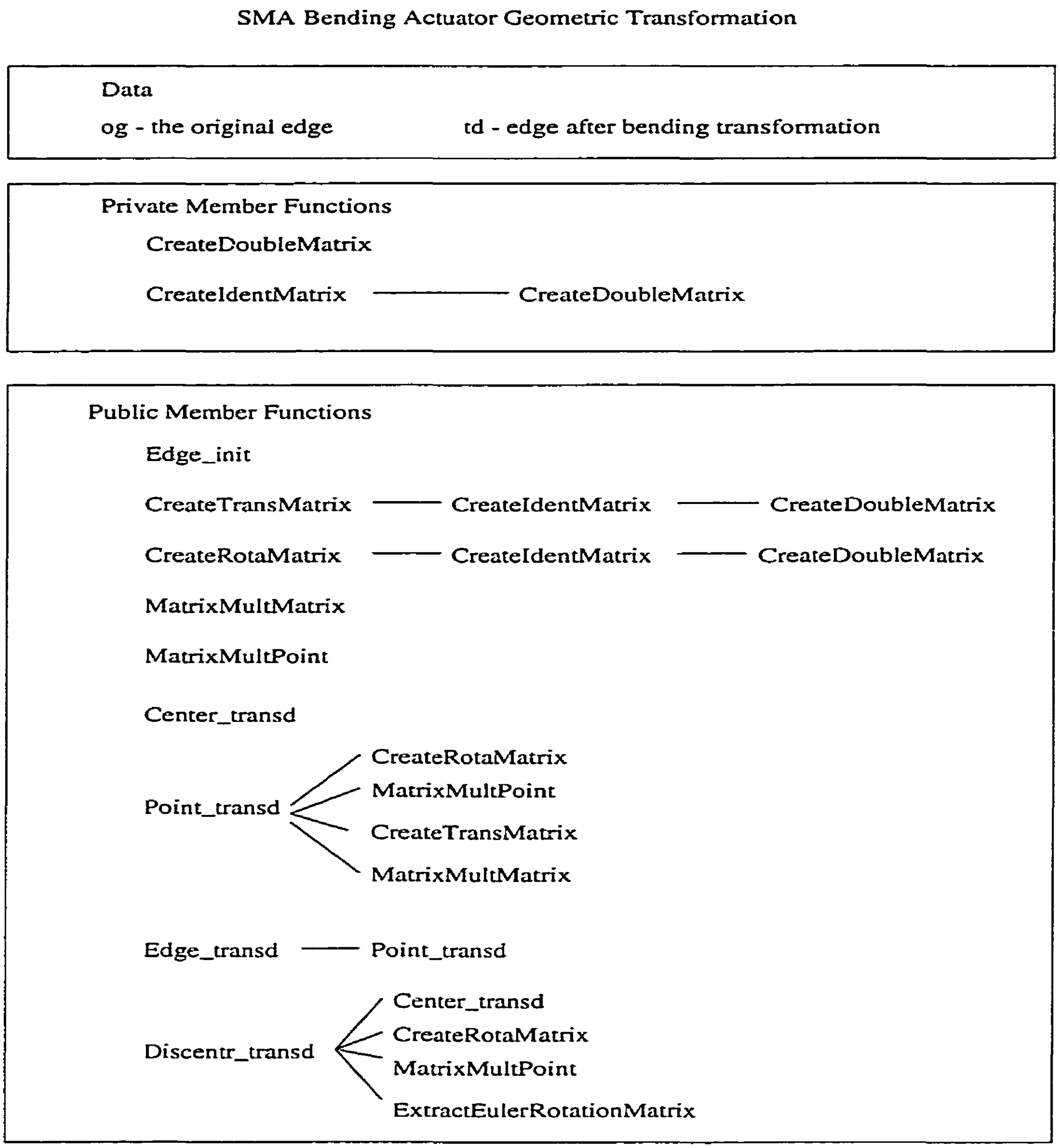

FIGURE B.7. SMA Bending Actuator Geometric Transformation Class

The Link List Class

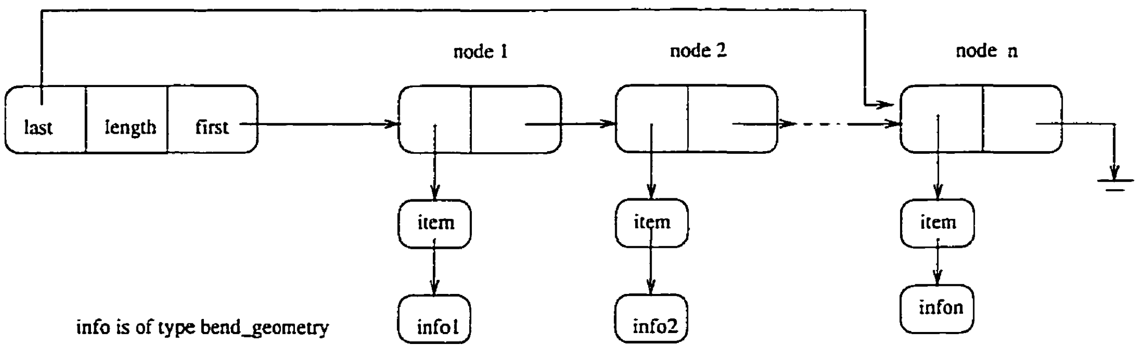

Data

length - the length of the link list

first - the address of the first node of the link list

last - the address of the last node of the link list

Public Member Functions

list

inst_node

InsertAtBegin —— inst_node

AppendToEnd —— inst_node

PrintList

get_length

get_firstnode

get_lastnode

FIGURE B.8. The Link List Class

REFERENCES

[1] Koji Ikuta, Masahiro Tsukamoto, and Shigeo Hirose, 1991, "Mathematical model and experimental verification of shape memory alloy for designing micro actuator", *Procs. of the IEEE MicroElectroMechanical Systems Conference*, pp. 103–108.

[2] T.W. Duerig, K.N. Melton, D. StHockel, and C.M. Wayman, 1990, "Engineering aspects of shape memory alloys", *Butterworth-Heinemann Ltd., Toronto.*

[3] K. Ikuta, 1990, "Micro/miniature shape memory alloy actuator", *Proc. of IEEE International Conference on Robotics and Automation*, pp. 2156–2161.

[4] S. Hirose, K. Ikuta, and Y. Umetani, 1984, "A new design method of servo actuators based on the shape memory effect", *Proc. of 5th RO.MAN.SY.symp. Udine, Italy*, pp. 339–349.

[5] D. Honma, Y. Miwa, and N.Iguchi, 1983, "Application of sme to digital control actuator", *Trans. JSME-C*, vol. 49(448), pp. 2163–2169.

[6] D. Grant and V. Hayward, 1995, "Design of shape memory alloy actuator with high strain and variable structure control", *Proc. of IEEE International Conference on Robotics and Automation*, vol. 3, pp. 2305–2312.

[7] D. Honma, Y. Miwa, and N. Iguchi, Oct. 1989, "Micro robots and micro mechanisms using shape memory alloy", *Integrated Micro Motion Systems, Micro-maching, Control and Application, Nissin, Aichi, Japan.*

[8] I.W. Hunter, S. Lafontaine, J.M. Hollerbach, and P. Hunter, 1991, "Fast reversible niti fibers for use in microrobotics", *Proceedings of the IEEE Micro-Electro Mechanical Systems Workshop, Aara, Japan*, pp. 166–170.

[9] R.A. Russell and R.B. Gorbet, 1995, "Improving the response of sma acctuators", *IEEE International Conference on Robotics and Automation*, pp. 2299–2304.

[10] R.B. Gorbet and D.W.L. Wang, 1995, "General stability criteria for a shape memory alloy position control system", *IEEE International Conference on Robotics and Automation*, pp. 2313–2319.

[11] K. Koehn and S. Payandeh, 1995, "Toward evaluation of shape memory alloy actuators for endosurgery", *Procs of the IEEE International Conference on Systems, Man and Cybernetics*, vol. 3, pp. 1991–1996.

[12] K. Ikuta, M. Tsukamoto, and S. Hirose, 1988, "Shape memory alloy servo actuator system with electric resistance feedback and application for active endoscope", *Proc. IEEE International Conference on Robotics and Automation*, pp. 427–430.

[13] H.F. Kaplan, 1995, "Steering borescopes with a shape memory alloy", *Photonics Spectra*, pp. 44–46.

[14] R.H. Sturges and S. Laowattana, 1993, "A flexible, tendon-controlled device for endoscopy", *The International Journal of Robotics Research*, vol. 12, pp. 121–131.

[15] T. Fukuda, S. Guo, K. Kosuge, F. Arai, M. Negoro, and K. Nakabayashi, 1994, "Micro active catheter system with multi degress of freedom", *Proc. IEEE International Conference on Robotics and Automation*, vol. 3, pp. 2290–2295.

[16] Danny Grant, 1995, "Shape memory alloy actuator with an application to a robotic eye", *Master's thesis, McGill University*.

[17] C. Liang and C.A. Rogers, 1992, "A multi-dimensional constitutive model for shape memory alloys", *Journal of Engineering Mathematics*, vol. 26, pp. 429–443.

[18] T.E. Buchheit, S.L. Kumpf, and J.A. Wert, 1992, "Modelling the stress-induced transformation behaviour of shape memory alloy single crystals", *Acta metall. mater.*, vol. 43, no. 11, pp. 4189–4199.

[19] M. Hashimoto, M. Takeda, H. Sagawa, and I. Chiba, 1985, "Application of shape memory alloy to robotic actuators", *Journal of Robotic Systems, 2(1):3-25.*

[20] K. Kuribayashi, 1986, "A new actuator of a joint mechanism using tini alloy wire", *The Int. Journal of Robotics Research, 4(4).*

[21] D.R. Madill, 1993, "Modelling and stability of a shape memory alloy position control system", *Master's thesis, University of Waterloo.*

[22] J. P. Holman, 1989, "Heat transfer", *McGraw-Hill Book Company, Toronto.*

[23] K. Ikuta, 1987, "The study on the shape memory alloy servo actuator", *Doctral Dissertation to Tokyo Institute of Technology.*

[24] D. Reynaerts and H. Van Brussel, 1991, "Development of a sma high performance robotic actuator", *Fifth International Conference on Advanced Robotics*, vol. 2.

[25] S. Ku and S.E. Salcudean, 1996, "Design and control of a teleoperated microgripper for microsurgery", *Procs. of IEEE International Conference on Robotics and Automation*, pp. 889–894.

[26] C.P. Chou and B. Hannaford, 1996, "Measurement and modelling of mckibben pneumatic artificial muscles", *IEEE Trancs on Robotics and Automation*, vol. 12, no. 1, pp. 90–102.

[27] J.D. Foley, 1996, "Computer graphics: principles and practice", *Reading, Mass. : Addison-Wesley.*

[28] Inc. Dynalloy, "Technical characteristics of flexinol actuator wires", brochure, Irvine, CA 92715.

Document Log:

Manuscript Version 0

Typeset by $\mathcal{A}\mathcal{M}\mathcal{S}$-LaTeX — 28 September 1997

XUEMEI LU

CENTER FOR INTELLIGENT MACHINES, MCGILL UNIVERSITY, 3480 UNIVERSITY ST., MONTRÉAL (QUÉBEC) H3A 2A7, CANADA,

E-mail address: alexandr@cim.mcgill.ca

Typeset by $\mathcal{A}\mathcal{M}\mathcal{S}$-LaTeX

IMAGE EVALUATION TEST TARGET (QA-3)

150mm

6"

APPLIED IMAGE, Inc
1653 East Main Street
Rochester, NY 14609 USA
Phone: 716/482-0300
Fax: 716/288-5989